広島大学学術情報リポジトリ
Hiroshima University Institutional Repository

Title	Seismic time-dependent resilience assessment of aging highway bridges incorporating the effect of retrofitting
Author(s)	Omidian, Pedram; Khaji, Naser; Aghakouchak, Ali Akbar
Citation	Structures , 63 : 106347
Issue Date	2024-04-04
DOI	
Self DOI	
URL	https://ir.lib.hiroshima-u.ac.jp/00056103
Right	© 2024. This manuscript version is made available under the CC-BY-NC-ND 4.0 license https://creativecommons.org/licenses/by-nc-nd/4.0/ This is not the published version. Please cite only the published version. この論文は出版社版ではありません。引用の際には出版社版をご確認、ご利用ください。
Relation	

Hiroshima University Institutional Repository

Seismic time-dependent resilience assessment of aging highway bridges incorporating the effect of retrofitting

Pedram Omidian[1], Naser Khaji[2,*], Ali Akbar Aghakouchak[1]

1 *Faculty of Civil and Environmental Engineering, Tarbiat Modares University, P.O. Box 14115–397, Tehran, Iran*

2 *Civil and Environmental Engineering Program, Graduate School of Advanced Science and Engineering, Hiroshima University, 1-4-1, Kagamiyama, Higashi-Hiroshima, Hiroshima 739-8527, Japan*

Abstract

Bridges are one of the most critical components of transportation networks, which are highly vulnerable due to exposure to natural hazards. In addition, multiple degradation mechanisms can considerably affect the functionality of highway bridges during their service life. Therefore, accumulated damage could also arise continuously because of seismic loading and structural deterioration, which consequently can change system resilience over its life-cycle. This study presents a probabilistic methodology to systematically evaluate and develop the time-dependent seismic resilience curves for Reinforced Concrete (RC) bridges under chloride attacks. In this regard, different jacketing materials with varying thicknesses are chosen for retrofitting purposes. In each case, the time-dependent seismic fragility curves (four damage states) for calculating the time-dependent seismic resilience curves are established through Probabilistic Seismic Demand Models (PSDMs) by performing Incremental Dynamic Analysis (IDA). Finally, the time-dependent seismic resilience curves are evaluated based on the time-dependent seismic fragility curves using the restoration function for all the retrofitting strategies by considering the effect of structural deterioration over

* Corresponding author. Telefax: +81-82-424-7790.

E-mail address: nkhaji@hiroshima-u.ac.jp (N. Khaji).

time. The results indicate that aging, earthquake intensities, and retrofitting strategies undeniably affect the time-variant seismic resilience of bridges, which is helpful for the long-term safety and reliability of bridges.

Keywords: Seismic time-dependent resilience; Infrastructures management; Aging bridge; Corrosion deterioration; Retrofitting strategies

1. Introduction

One of the most critical functions of infrastructure systems, such as transportation networks, is to provide essential services to communities and support their economic growth, security, and competitiveness. Bridges are one of the most common and critical components in the transportation network. Experiences from past earthquakes and the damage caused by these events have shown that bridges are one of the most vulnerable components of the transportation system as an infrastructure system [1]. In this regard, bridge damage during an earthquake can severely disrupt socio-economic activities, including Search and Rescue (SAR) operations, logistics, emergency routes for firefighting, and emergency evacuation routing. In order to reduce potential economic losses and human casualties during a seismic event, it is crucial to evaluate the performance of existing bridges and retrofit essential components such as piers. Accordingly, a reliable seismic vulnerability evaluation framework is becoming a high-priority demand for decision-makers to predict possible earthquake-induced damage in bridge networks [2-3]. It is an appropriate approach to find the best method to repair, maintain, retrofit, and evaluate the life-cycle of bridges [4].

Bridges are designed and constructed in various ways worldwide, so a single method cannot be used to assess the seismic vulnerability of highway bridges. Uncertainties, including different bridge components, material properties, and seismicity of the area, along with the need to better predict the seismic performance of bridges, have led to various vulnerability assessment methods for highway bridges [5-6]. Although each of these methods uses a specific mathematical framework to assess the vulnerability of bridges, the overall goal of seismic assessment of highway bridges is to ensure the safety and security of transportation network infrastructure and its acceptable functionality against seismic loads. In this respect, fragility curves have emerged as an essential decision-making support tool for identifying the relationship between hazards and structural and non-structural system features, as well as the consequences of damage during an event [7]. These curves indicate the probability of exceeding a particular damage state for varying hazard intensities. Therefore, fragility curves can provide information about the performance of infrastructure and determine its expected functionality in the event of a possible hazard such as an earthquake, and be effective in decision-making as a futuristic tool [8].

In general, there are four main methods for constructing seismic fragility curves: (1) an expert opinion-based method, (2) an empirical (or statistical)-based method, (3) an analytical (or simulation)-based method, and (4) a hybrid method [9-12]. The probabilistic damage distribution functions in the 1st and 2nd methods are presented based on experts' questioning and post-earthquake field observations/information, respectively. In the 3rd method, the main focus is on mathematically describing and creating a numerical structural model to assess the seismic risk of transportation networks. In the 4th method, empirical data and analytical modeling are combined to provide a more accurate and reliable approach for constructing fragility curves. In this line, Mander [13] was among the first researchers who studied the seismic fragility of highway bridges in the United States and proposed different approaches for constructing seismic fragility curves, which finally improved the reliability of fragility curves by providing a theoretical method. Lee et al. [14] estimated fragility curves for different classifications of highway bridges in Korea. The results revealed that different levels of damage in such structures did not depend only on the magnitude of the earthquake and the distance from the epicenter but also are a function of the site (in particular, soil type) and structural bridge characteristics. Wright et al. [15] examined the vulnerability of bridges in the central and southeastern US along with bridge retrofitting methods. Ghosh and Sood [16] proposed a framework for developing seismic fragility curves of deteriorating bridges under chloride-induced corrosion to improve time-dependent predictive functions, which can interpolate logistic regression coefficients for continuous seismic reliability evaluation during its life-cycle with reasonable accuracy. Biondini et al. [17] performed a series of Incremental Dynamic Analyses (IDA) to calculate the life-cycle resilience of aging Reinforced Concrete (RC) bridges in an illustrative transportation network under earthquake scenarios. In this respect, Panchireddi and Ghosh [18] proposed a novel index-based estimation methodology to calculate cumulative damage in highway bridges under repeated main shock sequences and corrosion deterioration during their service life. Shin et al. [19] discussed the need for developing a seismic performance-evaluation method for composite steel-concrete box girder bridges with aging piers by considering various seismic inputs and comparing the maximum displacement and maximum shear force responses of the piers. Messore et al. [20] investigated the increasing complexity of road infrastructures and bridge networks due to technological advancements and urban growth. Finally, they presented a life-cycle cost-based risk assessment approach for aging bridge networks. Han and Frangopol [21] proposed a life-cycle risk optimization management framework for existing bridge networks subjected to seismic hazards and corrosion.

As a result, the destructive effects of aging and structural corrosion are indicated in the time-varying seismic resilience of bridge networks. Resilience can be defined as the ability of a system to withstand the effects of disruptive events and efficiently recover to pre-event performance. Recently, there has been a great deal of interest in researching the field of bridge resilience as a sense-making tool for decision-makers [22-23]. In this line, Chen et al. [24] introduced a repair procedure-based recovery pattern to improve the estimation of structural seismic resilience. Chen et al. [25] proposed an optimization procedure to determine the optimal configurations of link beams in double-column tall pier bents, considering multiple performance objectives to enhance bridge seismic performance. Also, Chen et al. [26] investigated the seismic resilient design of tall bridge piers with rocking foundations using inerter-based systems, specifically focusing on using a tuned viscous mass damper system to minimize the tilt angle of the bridge pier. Zhong et al. [27] presented a novel hemisphere-based rocking hinge at the rocking interface to minimize local damage and facilitate construction. Omidian and Khaji [28] proposed a multi-criteria decision-making optimization framework for improving the seismic resilience of RC structures by selecting the retrofitting strategies optimized for the seismic resilience index and the cost of the retrofit. Also, Omidian and Khaji [29] introduced a comprehensive optimization framework for assessing the total life-cycle cost (LCC) and resilience using Genetic Algorithm (GA). This framework offers a systematic approach for decision-makers to choose the most suitable retrofit strategies that minimize the LCC while satisfying a given level of resilience.

One of the most critical steps in an infrastructure seismic risk mitigation plan is to identify an applicable methodology to assess its status incorporating various variables (e.g., the damage state of the structure, direct and indirect losses, and the level of functionality under hazard events during their service lifetime). As a risk indicator, seismic resilience is a driving concept in infrastructure systems' design, assessment, monitoring, maintenance, and management. In this connection, this research aims to present the interpolated log-normal distribution function parameters (i.e., the median and log-standard deviation) for calculating the time-dependent seismic resilience that considers the potential effects of aging on seismic vulnerability and the enhancement effect of retrofit on resilience curves/surfaces for different points in time. In addition, the deterioration mechanisms induced by corrosive chloride attack are evaluated by assuming a uniform corrosion scenario. The response of a typical five-span RC box girder bridge with different retrofitting strategies under other corrosion conditions and seismic scenarios is investigated to present the time-dependent seismic fragility and resilience curves. Fig. 1 graphically depicts the general view of the seismic resilience assessment framework of this study.

2. Background theories for disaster resilience

To implement the proposed methodology, the desired infrastructure should be selected in the first step, and potential natural hazards should be identified. The fragility curves are then calculated according to the type of structure and site characteristics. Finally, the resilience index is calculated based on the mentioned formulation. For different retrofit strategies and aging degradation, the general aforementioned steps are repeated, and the target objective (i.e., resilience) is evaluated. A simple and illustrative model is used to clarify the implementation steps of the seismic resilience assessment framework presented in this study. In this regard, an RC box girder bridge, one of the most critical transportation network components, is considered a case study infrastructure under corrosion.

2.1. Seismic resilience methodology (loss and recovery functions)

The measure of Resilience (R) encompasses various factors commonly used to assess overall seismic performance, such as restoration path, human fatalities, and economic losses. In this perspective, resilience (R) is the capability to sustain a predefined level of functionality $Q(t)$ during a control time (T_{LC}) for an infrastructure [29]. In this context, several studies have been conducted to practically define and calculate the resilience index of various infrastructure systems [30]. In this regard, the resilience index is defined analytically as [31]

$$R(t) = \int_{t_{0\mathrm{E}}}^{t_{0\mathrm{E}}+T_{\mathrm{LC}}} \frac{Q(t)}{T_{\mathrm{LC}}} \mathrm{d}t \tag{1}$$

As shown in Eq. (2), the analytical expression of the system functionality $Q(t)$ constitutes a loss function and a recovery function of infrastructure system performance during the period of system interruption because of the occurrence of an extreme event such as an earthquake. Mathematically, this term is given by the following equation

$$Q(t) = 1 - [L(I, T_{\mathrm{RE}}) \times \{H(t - t_{0\mathrm{E}}) - H(t - (t_{0\mathrm{E}} + T_{\mathrm{RE}}))\} \times f_{\mathrm{rec}}(t, t_{0\mathrm{E}}, T_{\mathrm{RE}})] \tag{2}$$

in which $L(I, T_{\mathrm{RE}})$ indicates the loss function as a function of hazard intensity (I) and the recovery time (T_{RE}) from the event E, and $f_{\mathrm{rec}}(t, t_{0\mathrm{E}}, T_{\mathrm{RE}})$ denotes the post-event recovery function. Also, $H(\cdot)$ represents the Heaviside (or unit) step function. The functionality (Q_0) can be measured in terms of a dimensionless cost (L_0), which is represented as $\left(\frac{\text{Cost of repair}}{\text{Replacement cost}}\right)$. Hence, the system resilience index or functionality right after any event ($t_{0\mathrm{E}}$) can be calculated as follows

$$R_0(\%) = Q_0 = 100 - L_0 = 100 - \sum_k P_E(LS_k).r_k \tag{3}$$

where k indicates the structural limit state (e.g., minor, moderate, major, collapse), and $P_E(LS_k)$ implies the probability of exceeding a structure limit state k after the event E. Additionally, r_k is the damage ratio associated with the kth limit state [32], which can be estimated as reported by FEMA [33].

It should be noted that some repair tasks should be established for the bridge to be rehabilitated through a given recovery path. Fu et al. [34] investigated the seismic performance of a bridge pier by identifying the critical elements in the repair effects. In addition, the estimates of the restoration functions (in the unit of time) are adopted by accounting for delays in decision-making, financing, and inspection, as outlined above, to evaluate the median time for recovery of highway bridge functions. In the case study structure of this research, the repair times dependence on the limit states is considered according to Fereshtehnejad and Shafieezadeh [35] for four limit states. Typically, as the severity of the damage increases, further time is needed to repair the damage and restore the structural condition to its original state (or intact state). In this line, Table 1 presents the recovery path for each seismic damage state, along with the corresponding probabilistic log-normal function for the required times. In this table, T_{ins} represents the time needed for the inspection and estimation, $T_{d\&c}$ denotes the required time for preparing a repair plan, bidding, and contracting, T_{mob} indicates the needed time for the mobilization of resources (including materials and crews), and T_{rep} signifies the time required for the repair.

2.2. Seismic fragility methodology (damage indices and states)

In this study, infrastructure system vulnerability or damage is measured by fragility curves. The fragility curves describe the likelihood of exceeding each damage state at varying levels of ground motion intensity measures. In a probabilistic seismic vulnerability assessment framework, the fragility of a system (or system component) is defined as the conditional probability $P_E(\cdot \mid \cdot)$ of demand being greater than the capacity [36]. To construct fragility curves, it is necessary to create a Probabilistic Seismic Demand Model (PSDM) that connects the Intensity Measure (IM) to the Engineering Demand Parameter (EDP). It should be noted that there are various Damage Indices (DIs) with different types of IM such as Peak Ground Acceleration (PGA), Peak Ground Velocity (PGV), Arias Intensity (AI), Spectral acceleration (Sa), Spectral displacement

(Sd) which are proposed by several studies. In this study, PGA is used as a suitable IM for large-scale seismic risk reduction plans to prioritize retrofit programs [37-41]. The "scaling approach" and the "non-scaling approach" can be used to create the PSDMs. The scaling approach generates the fragility curves by performing IDAs, which scale the ground motion to various levels. Alternatively, the cloud approach analyzes data without changing (or scaling) the ground motion's intensity level. The scaling approach is valuable for comprehending structures' inelastic behavior at different intensity scales. In general, the PSDMs are derived through regression analysis as

$$\ln(EDP) = \ln(a) + b\ln(IM) \tag{4}$$

in which a and b are regression coefficients obtained through the correlation between IM and EDP determined by incremental dynamic analysis. Considering the lognormal distribution to connect the EDP and the IM, the probability of exceedance of each damage state can be calculated using the following analytical relationship

$$P_E(D \geq DS_k|IM) = \phi\left[\frac{1}{\sigma_k}\ln\left(\frac{EDP}{\mu_k}\right)\right] \tag{5}$$

where $\phi[\,\cdot\,]$ is the log-normal cumulative distribution function with median value (μ_k) and log-standard deviation (σ_k) as the input fragility parameter for each damage state. DS_k represents the kth damage state (i.e., minor, moderate, major, collapse), respectively. It should be noted that generating fragility curves for individual bridge components, such as piers, bearings, and abutments, is a critical step in developing fragility curves for bridge systems. While some studies have focused on fragility curves for a single component (e.g., piers) and considered them sufficient for calculating system fragility, multicomponent fragility provides more robust results. In this study, the fragilities of three main components (i.e., piers, bearings, and abutments) are considered to construct the bridge system fragility. The probability of exceeding a certain level of damage for the entire bridge can be estimated by treating the bridge as a series system and applying the first-order boundary estimation method [42]. By utilizing

Eq. (6), the fragility probability of the bridge system can be estimated while considering the upper and lower bounds of damage probabilities [43]:

$$\max_{i=1:n}[P_E(\mathrm{comp}_i)] \leq P_E(F_{\mathrm{system}}) \leq 1 - \prod_{i=1}^{n}[1 - P_E(\mathrm{comp}_i)] \tag{6}$$

in which $P_E(\mathrm{comp}_i)$ indicates the exceedance probability of specific component damage state, and $P_E(F_{\mathrm{system}})$ characterizes the same for the bridge system.

In this study, various damage indices are considered for different bridge components. In this regard, the displacement ductility is adopted for bridge piers [42-43] as given below:

$$\mu_d = \frac{\Delta_u}{\Delta_y} \tag{7}$$

where Δ_u and Δ_y are the ultimate and yield displacements of piers, respectively. In addition, the damage states for the isolation bearings are determined using the capacity models outlined by Zhang and Huo [44] as bearing shear strain. Finally, the damage states for the abutments are specified using the capacity models proposed by Ramanathan [45] as abutment (active and passive) displacement. Many studies have widely utilized these damage states for different bridge components to evaluate the seismic fragility of bridges in regions with moderate to high seismic activity, encompassing both seismically and non-seismically designed bridges [46]. Table 2 presents the parameters needed to define the capacity models associated with different damage states (DS_k) for various components.

3. Modelling of case study bridge

Infrastructure systems include many single or multiple structures with simple to complex details. In order to illustrate the implementation steps of the proposed framework, a typical RC bridge model is employed to provide a clear demonstration of its practical application in seismic resilience assessment.

3.1. Bridge geometry and finite element modeling

The considered RC box girder bridge is adopted per the bridge model presented by Sultan and Kawashima [47]. This bridge is assumed to be a three-lane with five spans (two 39.6 m exterior spans and three 53.3 m interior spans). Fig. 2 provides additional details about the case study bridge modeled in the finite element SeismoStruct software [48], which also presents the specifications of pier sections.

This research uses nonlinear time-history dynamic analysis to determine the structure's response. For material nonlinearity modeling, the 3D inelastic Displacement-Based Element (DBE) is utilized to model the bridge piers. In addition, the fiber-based model is employed to generate the hysteretic relationship of the circular piers [49-50]. This element approximates the response by enforcing constant axial deformation and linear curvature distribution along its length. Hence, to improve the accuracy, especially in the plastic hinge region, the member is often divided into smaller lengths when using these elements. In the SeismoStruct [48], the cross-section behavior should be defined to accurately calculate the damage distribution in elements [51]. In this regard, the cross-section is divided into 400 fibers, each corresponding to a uniaxial stress-strain relationship. Next, the beam-column elements' stress-strain condition is determined by integrating the nonlinear uniaxial stress-strain response of the individual fibers. For dynamic time-history analyses, the Hilbert-Hughes-Taylor integration scheme is used to calculate the overall flexibility matrix of elements that considers the potential strain softening or localized deformations according to Fakharifar et al. [49] for FRP/steel jacketed RC bridge piers. The resulting forces and inelastic deformations are then distributed through fiber-based sections along the element length, with each section represented by an integration point. These fiber sections are assumed to remain plane throughout the analysis and satisfy strain compatibility between the longitudinal reinforcement and the surrounding concrete. Factors such as bond-slip deformations, shear deformations, P-delta effects, and strain rate effects on material properties are accounted for in the analysis [52].

The concrete material is modeled by a uniaxial nonlinear constant confinement model programmed by Madas [53] and initially developed by Mander et al. [54] for externally confined concrete. Also, this model considers a cyclic rule presented by Martinez-Rueda and Elnashai [55]. The reinforcement steel material is modeled using the uniaxial steel model initially programmed by Yassin [56] based on a simple yet efficient stress-strain relationship proposed by Menegotto and Pinto [57], coupled with the isotropic hardening rules proposed by Filippou et al. [58]. The current implementation follows that carried out by Monti et al. [59] and the memory rule suggested by Fragiadakis et al. [60] for higher numerical stability/accuracy under transient seismic loading. For retrofitting, the bridge piers are jacketed with three distinct materials (i.e., steel, Carbon Fiber-Reinforced Polymer (CFRP), and Glass Fiber-Reinforced Polymer (GFRP)) in this study, as summarized in Table 3.

The Fiber Reinforced-Polymer (FRP) material is considered a simplified uniaxial trilinear FRP model that assumes no compressive strength, which has linear elastic behavior up to the rupture with zero compressive strength [61]. CFRP and GFRP are modeled as TU27C-QuakeWrap and VU27G-QuakeWrap in SeismoStruct [48], which can consider different numbers of FRP layers. Both composite materials contain high-strength unidirectional fabrics, whose material properties are obtained from QuakeWrap Inc. product data sheets (Table 4). It should be noted that when the bridge pier is jacketed, the concrete cover is deemed as the concrete confined by the steel/FRP jacket in the presence of steel/FRP sheets that jacket the piers. In contrast, the core concrete is considered to be confined by the FRP and transverse reinforcements. In order to simulate the external confined concrete effect of FRP jacketing materials, Ferracuti and Savoia's model [62] is implemented, which follows the constitutive relationship and cyclic rules proposed by Mander et al. [54] and Yankelevsky and Reinhardt [63] under compression and tension, respectively. This FRP-confined concrete model adheres to the constitutive relationship and cyclic rules under compression and tension states, respectively. Regarding the properties of the steel jacket material, a uniaxial bilinear stress-strain model with kinematic strain hardening is utilized, as outlined in Table 4.

Steel jackets of four different thicknesses (T1 to T4) of 9.53, 12.7, 19.05, and 25.40 mm are selected for pier retrofitting. Furthermore, the piers are jacketed with 2, 4, 7, and 10 plies of CFRP and GFRP with 1.24 and 1.27 mm thicknesses for each ply, respectively. Table 4 represents the specifications of the materials considered in this study. Additionally, eight different arrangements of the piers of the bridge are considered for the retrofit designs in four categories (namely, Full (F), Three quarter (Tq), Half (H), and Quarter (Q)), as shown by red and black diagonal strips in Fig. 3, in which short names indicate the retrofitting arrangements. Moreover, various retrofitting strategies are assessed using three materials with different plies' thicknesses and numbers, and the resilience index and LCC are determined for each scenario.

3.2. Incremental dynamic analysis and ground motion data

In the seismic vulnerability assessment of structures, fragility curves are commonly obtained through the IDA, which can be used to calculate the resilience curves/surfaces. In this method, each Strong Ground Motion (SGM) record is scaled into a wide range of seismic intensity levels and monotonically applied to the case study structure to extract different structural damage states from elastic to collapse. Therefore, a critical factor in the nonlinear dynamic analysis of structures is the selection of a sufficient number of appropriate SGMs, as the results of the analyses heavily rely on the input ground motion [64]. In this line, Shome and Cornel [65] suggested that using 10 to 20 records can yield reliable estimates of structural response. For this reason, 20 time-histories are considered from the Pacific Seismic Engineering Research (PEER) database [66] for IDAs. Table 5 presents the SGM data corresponding to an earthquake magnitude of approximately 5.5~7.5 and the typical soil classification (i.e., $360 \leq V_{S30} \leq 760$ m/s). It should be noted that each record is scaled into ten stages from PGA = 0.1g to 1.0g by an incremental step of 0.1g [29]. Assuming a damping ratio of 5%, the acceleration response spectra of 20 earthquake records are shown along with their mean amplitudes in Fig. 4.

3.3. Bridge components degradation due to corrosion

As mentioned, one of the objectives of this study is to investigate the effect of deterioration on seismic resilience. In general, the strength of different components of a structure changes during its service life and decreases due to factors such as corrosion, erosion, other forms of chemical deterioration, and fatigue [69]. In this regard, highway bridges are often exposed to harsh environmental conditions. They will deteriorate if not correctly maintained over time, affecting their functionality under seismic hazard events. In this line, one of RC bridges' most critical and vulnerable elements is their piers, which are exposed to chloride-induced corrosion. Therefore, consideration of this factor can be crucial in resilience-based decision frameworks. In the following, it is discussed how to consider the degraded model for the under-study bridge.

In general, corrosion of reinforcing steel can be assigned to the penetration of chloride ions that pass through the concrete surface cover and cause degradation. Therefore, small individual pits or cracks on the steel bar are developed during the corrosion propagation stage. Over time, these pits and cracks expand and cause wider cracks in the form of uniform corrosion [70]. It should be noted that the corrosion tends to develop uniformly on the reinforcing bars in carbonated concrete without relevant chloride content, as depicted in Fig. 5(a) [71]. In this study, it is assumed that there is a traffic spray scenario in which the de-icing of salt chlorides gets airborne because vehicles pass through chloride-laden water under the bridge. In addition, it is assumed that the reinforcement steel area loss due to corrosion occurs uniformly along the length of the pier, as uniform corrosion [72]. Also, the non-uniform pitting corrosion of steel reinforcing bars in a chloride environment is excluded in the present study for simplicity. However, this study explicitly considers other effects of non-uniform pitting corrosion, such as the reduction in steel strength and ductility according to the recommendations of Dizaj et al. [73].

As a result, Fick's second law of diffusion [74] through a semi-infinite solid can be used to simulate the penetration of chloride ions into RC structures as follows [75]

$$\frac{\partial C(x,t)}{\partial t} = -D_c \frac{\partial^2 C(x,t)}{\partial x^2} \tag{8}$$

in which C and D_c indicate chloride ion concentration and diffusion coefficient, respectively. Also, x represents the depth of concrete from the surface. If the concentration of chloride ions near the concrete surface is assumed to be constant (like that usually assumed for corrosion due to de-icing salts), the corrosion initiation time (T_i) can be estimated by the following relation [76]

$$T_i = \frac{x^2}{4D_c}\left[\mathrm{erf}^{-1}\left(\frac{C_0 - C_{cr}}{C_0}\right)\right]^{-2} \tag{9}$$

where C_0 and C_{cr} are equilibrium chloride concentration at the concrete surface and critical chloride concentration that causes the dissolution of the passive protective film around the reinforcement and initiates corrosion, respectively. Additionally, erf (θ) denotes the Gaussian error function, which analytically is defined as

$$\mathrm{erf}\,(\theta) = \frac{2}{\sqrt{\pi}}\int_0^{\theta} \exp(-p^2)\,\mathrm{d}t \tag{10}$$

It is important to highlight that the start time of corrosion (i.e., T_i) relies on various parameters, such as the bridge's location and environmental conditions, which can vary. Therefore, it is necessary to use probabilistic models to consider such uncertainties following Table 6 [77]. Hence, when the passive protective layer around the reinforcement dissolves due to the constant attack of chloride, corrosion begins, and the loss of time-dependent reinforcement cross-section, $A(t)$, can be obtained by [75-76]

$$A(t) = \begin{cases} n_{\text{bars}} D_i^2 \frac{\pi}{4} & \text{for } t \leq T_i \\ n_{\text{bars}} [D(t)]^2 \frac{\pi}{4} & \text{for } T_i < t < T_i + D_i / r_{\text{corr}} \\ 0 & \text{for } t \geq T_i + D_i / r_{\text{corr}} \end{cases} \tag{11}$$

in which n_{bars} indicates the total number of reinforcement bars, and t represents the elapsed time in years. In addition, D_i denotes the initial diameter of steel reinforcement, and $D(t)$ is the steel reinforcement diameter at the end of time $t - T_i$, with the rate of corrosion r_{corr}. Furthermore:

$$D(t) = D_i - r_{\text{corr}}(t - T_i) \tag{12}$$

In this study, the corrosion rate during the life-cycle of the bridge based on previous studies is assumed to be constant due to the lack of detailed data for time-dependent corrosion rate. However, this rate can be variable according to environmental conditions [78]. As mentioned earlier, the uncertainty about the corrosion rate is calculated by a probabilistic model instead of a single deterministic value based on Table 6. In this context, the area of the reinforcing steel at time t, $A(t)$, normalized by the initial size of the reinforcement, A_i, as time-dependent area reduction ratio is shown in Fig. 5(b). In addition, the red dashed lines show the Probability Density Functions (PDFs) for corrosion parameters, and the black curve indicates the mean values of normalized time-variant area reduction of the RC pier reinforcement. As seen from Fig. 5(b), it shows the reduction of the steel cross-sectional area during the considered timespan and the increase of uncertainty regarding the estimation of the reinforcement area due to the combined effect of the corrosion initiation time T_i, the variability of the corrosion rate r_{corr}, and the initial diameter of the reinforcement D_i. The loss of steel area due to corrosion of RC piers is correspondingly modeled as a reduction in the cross-sectional area of the longitudinal reinforcing bar in the fiber section model compared to the intact piers in the finite element model. This study considers the effect of structural deterioration at 0 (i.e., intact case), 25, 50, 75, and 100 years. In this study, the structural deterioration is assumed to naturally initiate after applying retrofitting strategies on the bridge system of the retrofitted case. This assumption implies that the retrofitting measurements implemented on the bridge system will effectively restore the structural performance to its initial state or even enhance it [79]. Therefore, the time of applying the retrofitting is considered the base scenario for the retrofitted case. In other words, any deterioration or damage that occurs after the retrofitting (i.e., 0 year for the intact case) is assumed to be due to external factors. Also, the effect of FRP layers on aging RC columns is considered following Dhakal [79] (for further discussions, refer to [80-82]). Since FRP layers are corrosion resistant, enhancing structures' durability [81, 83], the deterioration of FRP layers is not considered in the modeling. It should be noted that in addition to the loss of reinforcement cross-section, corrosion deterioration can give rise to various secondary consequences. These include the reduction of the strength of both the concrete cover and core, as well as a reduction in the strength and ductility of the steel. The secondary effects of corrosion deterioration examined in this study are outlined below.

3.3.1. Secondary effects of corrosion deterioration

The corrosion deterioration process generates splitting stresses caused by the expansion of rust products, ultimately forming micro-cracks in the concrete cover. These cracks can potentially widen over time, eventually resulting in the spalling or detachment of the cover. The assessment of the concrete cover strength is carried out according to the methodology proposed by Biondini and Vergani [71] as given by:

$$f_c(t) = f_{ci} \left(1 + K \frac{n_{\text{bars}}\, w_{cr}(t)}{\varepsilon_{ci}\, D_i}\right)^{-1} \tag{13}$$

where $f_c(t)$ indicates the time-dependent strength of the spalling and cracking concrete cover, and f_{ci} and ε_{ci} are the initial strength and strain of the non-corroded concrete cover, respectively. The parameter K is assumed to be 0.1, which is associated with the diameter of steel reinforcement and its roughness [72]. In addition, $w_{cr}(t)$ implies the total crack width at time t, which can be calculated by the available empirical formula and depends on the depth of corrosion attack and volumetric expansion of corroded rebars [84]. In this line, the variation of mean cover concrete strength $f_c(t)$, normalized by the initial concrete cover strength f_{ci}, as time-dependent strength reduction ratio is shown in Fig. 5(c).

Besides the loss of strength in the cover concrete, corrosion deterioration also results in a decrease in the strength of the core concrete due to the loss of area of transverse ties. To evaluate the reduced confined core concrete strength, the model initially introduced by Mander et al. [54] and developed by other researchers for aging columns [85] is utilized in this study as follows:

$$f_{cc}(t) = f_{ci} \left(-1.254 + 2.254 \sqrt{1 + \frac{7.94 f_{cl}(t)}{f_{ci}}} - 2 \frac{f_{cl}(t)}{f_{ci}}\right) \tag{14}$$

in which $f_{cc}(t)$ indicates the time-dependent strength of the confined core concrete. Also, $f_{cl}(t)$ is the effective lateral confining stress distributed over the surface of the core concrete. It is defined by a function of the volumetric ratio of transverse tie reinforcement, which undergoes a time-dependent reduction due to corrosion deterioration. As mentioned earlier, the corrosion deterioration along the length of the rebar causes a decrease in the yield or ultimate strength and ductility of the steel reinforcement. Experimental studies conducted on bare or reinforced steel bars have demonstrated that the strength of the steel decreases linearly with the loss of mass [86]. In this regard, the percentage mass loss of steel $X(t)$, due to corrosion at time t can be calculated by the following relation:

$$X(t) = \frac{A_i - A(t)}{A_i} = \frac{{D_i}^2 - D(t)^2}{{D_i}^2} \tag{15}$$

The yield or ultimate time-dependent strength of the corroding steel reinforcement at time t can be estimated as:

$$f_{sy}(t) = [1 - 0.005X(t)]f_{si} \tag{16}$$

where f_{si} is the corresponding yield or ultimate strength of the non-corroded reinforcement.

The reduction in steel ultimate strain does not conform to a linear model, as indicated by various experiments reporting a wide range of strain reduction values [87]. Consequently, this study adopts the experimental findings of Apostolopoulos and Papadakis [88], who observed a nonlinear relationship between ultimate strain and percentage mass loss. According to the analysis of experimental data, the ultimate strain is correlated with the percentage mass loss based on the equation proposed by Biondini and Vergani [71] as follows:

$$\varepsilon_{su}(t) = \begin{cases} \varepsilon_{sui} & \text{for } 0 \leq X(t) < 1.6 \\ 0.1521\varepsilon_{sui}[X(t)]^{-0.4583} & \text{for } 1.6 \leq X(t) \leq 100 \end{cases} \tag{17}$$

in which ε_{sui} and $\varepsilon_{su}(t)$ correspond to the ultimate strain of the non-corroded and corroding reinforcements, respectively.

4. Seismic resilience development methodology

The probabilistic seismic demand models should be determined in the first step to assess the time-dependent seismic resilience. To achieve this purpose, a series of IDAs is conducted for each retrofitting strategy. Next, fragility curves are determined for each of the four damage states (i.e., minor, moderate, major, collapse) using calculated PSDM at a range of seismic intensity levels from PGA = 0.0 to PGA = 1.0g. Finally, time-dependent seismic resilience curves/surfaces are calculated for each aging case, retrofitting arrangements with different materials and thicknesses following the explained assumptions and formulation in section 2.

4.1. Probabilistic seismic demand models

The Probabilistic Seismic Demand Models (PSDMs) can establish a statistical relationship between the median peak seismic response of critical bridge components and the seismic intensity. This study considers the PGA and the three components (i.e., pier displacement ductility, bearings shear strain, and abutment displacement) of the bridge system as the seismic intensity and engineering demand parameter, respectively. The PSDMs are developed by the IDA when these critical elements are exposed to chloride-induced corrosion at 0 (intact or pristine case), 25, 50, 75, and 100 years of service life [89]. At each point, 20 SGMs from the ground motion ensemble are paired with statistically similar bridge samples that reflect uncertainties in modeling, material variables, and deterioration parameters. The probabilistic seismic demand models for RC piers for the pristine case and different retrofitted strategies bridge are shown in Fig. 6. In each panel, the lines represent the linear regression relationship of the form given in Eq. (4), and the top line (indicated by a solid blue line) marks the non-retrofitted bridge. In contrast, the lowermost line (shown by a solid black line) indicates retrofitted with the thickest considered material and arrangement. At the same time, the markers depict the ground motion intensity and EDP for highlighted cases. As seen from the results from Fig. 6, different PSDMs arise based on various strategies (i.e., different retrofitting jacketing materials, thicknesses, and arrangements). In this line, materials with more strength, such as CFRP, can remarkably reduce structural responses against seismic loads. This ability increases by using strategies that retrofit more piers with thicker material. Also, the influence of aging is examined and demonstrated in Fig. 7.

By comparing the results from Fig. 6 and Fig. 7, the median estimates of seismic demand based on the PSDMs are increased according to two main factors: (1) over time from pristine to corrosion conditions and (2) different seismic intensities. This can be attributed to the higher uncertainty in determining the degree of deterioration and how the bridge responds to SGMs. In this regard, it should be noted that retrofitting has a significant effect on reducing the seismic vulnerability of bridges by considering the effect of corrosive chloride attack as structural deterioration. Generally, this effect can be presented in two categories as follows:

(I) With retrofitting under the effect of corrosion, the median values of the responses (or linear regression relationship between IM and EDP) are significantly reduced compared to retrofitting without aging and the non-retrofitted case.

(II) Retrofitting strategies in which a greater number of bridge piers are retrofitted with more strength and thicker materials lead to an increase in this effect (see Fig. 7(b) and Fig. 7(d)).

4.2. Time-dependent seismic fragility curves development

To achieve the time-dependent seismic resilience curves, it is necessary to measure time-dependent seismic fragility curves based on the probabilistic seismic demand models described in the previous section. The fragility curves indicate the probability of damage to the studied system for different damage states and the effects of different ground motion intensity levels, which can lead to a better understanding of the seismic vulnerability of bridges under various uncertainties. In this line, curve fitting is used to find the best fit curve representing a set of data points. In the case of fragility curves, curve fitting models the relationship between an input parameter (such as ground motion intensity) and the probability of exceeding a specific damage state or performance level. To accomplish this, a mathematical function that accurately describes the connection between the independent variable (hazard intensity) and the dependent variable (probability of damage) needs to be identified. The lognormally curve fitting method is commonly used to develop fragility curves [90]. The first step in this method involves collecting data on the damage or performance of structures for different hazard intensity levels. This data is then transformed into a logarithmic scale, as a log-normal distribution appears symmetrical when portrayed on this scale. The transformed data is then plotted on a scatter plot, with the logarithmic hazard intensity on the x-axis and the quantile of damage on the y-axis. The curve is typically represented by the median and percentile values, such as the 16th, 50th, and 84th percentiles (corresponding to one standard deviation away from the median).

To evaluate the impact of corrosion on seismic vulnerability, the time-dependent seismic fragilities of the bridge system are calculated at different times during their life-cycle, following the general expression of seismic fragility in section 2.2. In this process, the probability of structural damage at four damage states (i.e., minor, moderate, major, collapse) is calculated for non-retrofitted bridges under different years of corrosion (i.e., pristine, 25, 50, 75, and 100 years), as illustrated in Fig. 8.

The results of Fig. 8 indicate that the fragility curves generally increase over time as the bridge corrosion continues. It can be observed that for a specific intensity level (namely, the PGA), the bridge system tends to have a higher median damage index for corrosion conditions compared to the pristine case. However, the increase rate of the probability of structural damage varies according to seismic intensity, damage state, and the duration of deterioration. In line with the results, the probability of structural damage increases at higher seismic intensities. For example, with PGA = 0.3 g, there is approximately a 10.4% and 15.2% chance of achieving a moderate damage state for the pristine and 50 years aging cases, respectively, while under the PGA = 0.6 g and the same damage state, these values are nearly equal to 45.9% and 55.1% (Fig. 8(b)). In addition, this difference in fragility values increases with the change of damage state from minor to collapse (Fig. 8(a-c)) and more exposed to harsh environmental conditions (i.e., from 0 to 100 years) (Fig. 8(d)). Also, the influence of retrofitting is depicted in Fig. 9.

As seen in Fig. 9, different retrofitting strategies effectively reduce the vulnerability of aging bridges. In this regard, various arrangements with different materials and thicknesses have different effects on reducing vulnerability. Materials with higher strength, such as CFRP, more retrofitted piers, and the number of layers/thicknesses, are more efficient in lowering vulnerability (Fig. 9(a - b)), consequently increasing the resilience index. In each panel of this figure, the topmost curve (indicated by a solid black line) represents the non-retrofitted structure. In contrast, the lowermost curve indicates the most efficient approach for mitigating damage. In all cases, the lowermost curves correspond to the cases where all piers are covered with the thickest jacketing. In addition, retrofitting reduces the destructive effect of structural deterioration (Fig. 9(a) and Fig. 9(c)). Also, the effectiveness of retrofitting strategies increases when the damage state goes from minor to collapse and under severe seismic intensities (Fig. 9(c - d)). In general, fragility curves for retrofitted bridges are less varied than those of non-retrofitted structures, which makes the structure more stable against the aforementioned damaging factors.

4.3. Time-dependent seismic resilience curves development

In disaster management, a reliable, robust, and efficient index is necessary for decision-makers to prepare crisis management strategies (including mitigation, preparedness, response, and recovery phases) by considering the current, during, and post-event infrastructure under hazard events. In this regard, the seismic resilience index can establish a sense-making relationship between the functionality level of the under-study infrastructure and the potential seismic intensity. It can provide an overview of the infrastructure's status before, during, and post-earthquake events over time by considering and applying fitted recovery paths on the system's situation. In this study, the time-dependent seismic resilience curves are evaluated for all the retrofitting strategies by considering the effect of structural deterioration over time, as mentioned in section 2.1. The time-dependent seismic resilience surfaces are calculated using the restoration function based on the time-dependent seismic resilience curves. Fig. 10 illustrates the time-dependent seismic resilience curves for the selected arrangements and materials by considering all discussed assumptions and related formulations in section 2.

As observed from the results in Fig. 10, the seismic resilience index decreases with the continuation of corrosion and increases in seismic intensity at different rates based on the type of retrofitting strategy and the time of deterioration. In this respect, retrofitting action leads to an improvement in the resilience index compared to the non-retrofitted structure so that the mentioned destructive effect of seismic intensity can be significantly reduced (evident in Fig. 10(a - b)). These results underline the importance of considering the impact of aging on the response of bridge systems. In addition, materials such as CFRP with high strength combined with robust retrofitting strategies (i.e., a greater number of retrofitted piers and thickness) have a notable influence on enhancing the resilience index (Fig. 10(b - c)). Moreover, their significant effect in mitigating the destructive consequences of aging becomes more pronounced as corrosion conditions worsen from pristine to 100 years (Fig. 10(c - d)). Table 7 represents the median and log-standard deviation values of the interpolated log-normal distribution functions for the system's resilience immediately following seismic hazard events at different aging time intervals. For a better comparison of the obtained results, the Retrofit Efficiency (RE) ratio is defined as the ratio of "useful output" to "total input" for the seismic resilience index as follows:

$$RE(\%) = \frac{\text{Useful output}}{\text{Total output}} \times 100\% \quad (18)$$

where the useful output denotes the amount of increase in the seismic resilience index due to retrofitting compared to the non-retrofitted situation. In addition, the total input indicates the seismic resilience index of the non-retrofitted situation. Fig. 11 plots the RE for different CFRP jacketing strategies and aging conditions. Also, Table 8 presents the percentage increase in the median of the log-normal distribution function of system resilience that can be attained by various retrofitting designs. In this table, the percentage increase is fitted as exponential functions based on two ratios as general categories: (1) assuming that the arrangement is fixed and examining the effect of different thicknesses, and (2) assuming that the thickness is constant and investigating the effect of different retrofit arrangements.

As mentioned, the resilience of the desired structure is dropped just after a seismic hazard event occurs. It can then be restored to its intact state through repair actions. Mathematically, this drop in resilience and the effect of recovery measurement on it can be calculated by utilizing the Heaviside step (or the unit step function) and restoration functions, as illustrated in Fig. 12. The results show that the effect of structural deterioration on the seismic resilience is meaningful so that it decreases seismic resilience with a higher rate compared to a pristine state. In addition, this effect is magnified in a severe earthquake, which causes the structure's restoration to be affected (Fig. 12(a-b)). On the other hand, it is possible to deal with the destructive effects of the deterioration of the structure and the seismic risk by retrofitting the structure, as shown in Fig. 12(c-d). In this connection, the appropriate retrofitting strategy can provide more stable conditions for the infrastructure before, during, and post-hazardous events.

5. Conclusions

This study focuses on evaluating the impact of aging on the seismic resilience of highway bridges as one of the critical elements in the transportation network. In this regard, a simplified probabilistic framework is presented to determine and develop the corroded bridge's time-dependent seismic resilience over time by assuming uniform corrosion. For this purpose, a typical RC box girder bridge is investigated in detail as a case study infrastructure. Fragility curves are constructed for each aging scenario (i.e., including a non-retrofitted and retrofitted bridge system with different strategies) based on the PSDMs by employing IDAs. Finally, time-dependent seismic resilience curves are constructed for each aging scenario. Specific results obtained from this research are as follows:

- The PSDMs for under-study bridge are increased as the corrosive chloride attack and seismic intensities increase. However, different retrofitting strategies in RC bridge piers can significantly reduce their seismic vulnerability by considering the effects of aging at different rates. In this regard, increasing the strength and thickness of materials in the retrofitting process further enhances this ability.
- The comparison of the calculated time-dependent seismic fragility curves indicates that they increase over time with different rates as corrosion continues, primarily influenced by three factors: (1) higher seismic intensity input, (2) transitions in damage states from minor to collapse, and (3) the duration of deterioration ranging from 0 to 100 years. In this respect, retrofitting actions are very effective in further

stabilizing the structure against the combined destructive effects of seismic hazard and deterioration. Additionally, this reliability can be increased by applying retrofitting strategies on the bridge that include materials with higher strength, more retrofitted piers, and more the number of layers, which ultimately leads to an increase in the resilience index.

- The time-dependent seismic resilience surfaces are calculated for all the retrofitting strategies under different seismic scenarios by considering the effect of aging over time. The results indicated that the seismic resilience index decreases at different rates depending on the continuation of corrosion and the increase in seismic intensity. In this line, retrofitting interventions increase the resilience index compared to the non-retrofitted structure and significantly mitigate the simultaneous destructive effect of seismic intensity and aging. In addition, robust retrofitting strategies (such as incorporating more retrofitted piers and thickness) have a more remarkable impact on increasing the resilience index and RE ratio, thereby neutralizing the aforementioned destructive effects.
- Finally, The median and log-standard deviation values of the interpolated log-normal distribution functions are presented to quantify the bridge system resilience after seismic hazard events by incorporating the effects of different aging time and retrofitting strategies. The suggested statistical/mathematical functions are based on the PGA as the main intensity measure in seismic hazard analysis. These functions can aid decision-makers in preparing optimal strategies for crisis management, including mitigation, preparedness, response, and recovery phases.

Appendix A

In order to validate the accuracy and reliability of the outcomes derived from the modeling conducted via the SeismoStruct software [48], a nonlinear time-history analysis is undertaken. This analysis aims to assess the behavior of an actual RC bridge pier subjected to a uniaxial SGM based on the study conducted by Bianchi et al. [91]. Fig. A1(a) illustrates the actual model installed on the shaking table. At the same time, Figure A1(b - c) compares the responses of base shear and top displacement for the bridge pier simulated using the SeismoStruct and the results obtained from the shaking-table experiment. Obviously, there is a close alignment between the numerically predicted and experimentally measured time-history data for both top displacement and base shear responses.

Acknowledgments: The authors would like to thank four anonymous reviewers for their fruitful discussions and comments on the manuscript.

References

[1] Barros, B., Conde, B., Cabaleiro, M., & Riveiro, B. (2023). Deterministic and probabilistic-based model updating of aging steel bridges. *Structures*, 54, 89-105. DOI: 10.1016/j.istruc.2023.05.020

[2] Uenaga, T., Omidian, P., George, RC., Mirzajani, M., & Khaji, N. (2023). Seismic resilience assessment of curved reinforced concrete bridge piers through seismic fragility curves considering short- and long-period earthquakes. *Sustainability*, 15(10), Article 7764. DOI: 10.3390/su15107764

[3] Kim, J-S., Park, W-S., & Han, T-S. (2021). Framework to evaluate seismic fragility of bridges considering component damage correlations. *Journal of Earthquake and Tsunami*, 15(5), Article 2150022. DOI: 10.1142/S1793431121500226

[4] Leiva-Maldonado, S., Bowman, DM., & Gomez, D. (2023). Life-cycle cost profiles selection for different superstructure bridge types. *Structures*, 54, 1-13. DOI: 10.1016/j.istruc.2023.04.105

[5] Apandi, NM., Ma, Ch-Kh., Chin, CH-L., Awang, AZ., Rashid, ASA., & Zailani, WWA. (2023). Preliminary pre-damaged level assessment for concrete structures: A review. *Structures*, 54, 1381-1390. DOI: 10.1016/j.istruc.2023.05.130

[6] Zhao, B., Ho, J., Banerjee, S., Goh, S-H., & Lee, F-H. (2022). Modeling seismic-soil-pile interaction (SSPI) problems for large pile groups. *Journal of Earthquake and Tsunami*, 16(3), Article 2240005. DOI: 10.1142/S179343112240005X

[7] Mo, R., Chen, L., Xing, Zh., Ye, X., Xiong, Ch., Liu, Ch., & Chen, Y. (2023). Bridge seismic fragility model based on support vector machine and relevance vector machine. *Structures*, 52, 768-778. DOI: 10.1016/j.istruc.2023.03.179

[8] Pahlavan, H., Zakeri, B., & Ghodrati Amiri, Gh. (2017). probabilistic performance assessment of retrofitted horizontally curved multi-frame RC box-girder bridges. *Journal of Earthquake and Tsunami*, 11(4), Article 1750010. DOI: 10.1142/S1793431117500105

[9] Razzaghi, MS., Safarkhanlou, M., Mosleh, A., & Hosseini, P. (2018). Fragility assessment of RC bridges using numerical analysis and artificial neural networks. *Earthquakes and Structures*, 15(4), 431-441. DOI: 10.12989/eas.2018.15.4.431

[10] Karimi-Moridani, K., Zarfam, P., & Ghafory-Ashtiany, M. (2020). A novel and efficient hybrid method to develop the fragility curves of horizontally curved bridges. *KSCE Journal of Civil Engineering*, 24(2), 508-524. DOI: 10.1007/s12205-019-0217-9

[11] Sandoli, A., Lignola, GP., Calderoni, B. & Prota, A., (2021). Fragility curves for Italian URM buildings based on a hybrid method. *Bulletin of Earthquake Engineering*, 19, 4979-5013. DOI: 10.1007/s10518-021-01155-4

[12] Liu, Zh., Sextos, A., Guo, A., & Zhao, W. (2022). ANN-based rapid seismic fragility analysis for multi-span concrete bridges. *Structures*, 41, 804-817. DOI: 10.1016/j.istruc.2022.05.063

[13] Mander, JB. (1999). Fragility curve development for assessing the seismic vulnerability of highway bridges. Multidisciplinary Center for Earthquake Engineering Research, University at Buffalo, State University of New York.

[14] Lee, SM., Kim, TJ., & Kang, SL. (2007). Development of fragility curves for bridges in Korea. *KSCE Journal of Civil Engineering*, 11, 165-174. DOI: 10.1007/BF02823897

[15] Wright, T., Desroches, R., & Padgett, JE. (2011). Bridge seismic retrofitting practices in the central and southeastern United States. *Journal of Bridge Engineering*, 16(1), 82–92. DOI: 10.1061/(ASCE)BE.1943-5592.0000128

[16] Ghosh, J., & Sood, P. (2016). Consideration of time-evolving capacity distributions and improved degradation models for seismic fragility assessment of aging highway bridges. *Reliability Engineering & System Safety*, 154, 197–218. DOI: 10.1016/j.ress.2016.06.001

[17] Biondini, F., Capacci, L., & Titi, A. (2017). Life-cycle resilience of deteriorating bridge networks under earthquake scenarios. *16th World Conference on Earthquake,* 16WCEE, Santiago Chile, January 9th to 13th, Paper No. 939.

[18] Panchireddi, B., & Ghosh, J. (2019). Cumulative vulnerability assessment of highway bridges considering corrosion deterioration and repeated earthquake events. *Bulletin of Earthquake Engineering*, 17(3), 1603-1638. DOI: 10.1007/s10518-018-0509-3

[19] Shin, S., Hong, JY., Moon, J., & Song, JK. (2020). Seismic response evaluation of composite steel–concrete box girder bridge according to aging effect of piers. *Journal of the Computational Structural Engineering Institute of Korea*, 33(5), 319-329. DOI: 10.7734/COSEIK.2020.33.5.319

[20] Messore, MM., Capacci, L., & Biondini, F. (2021). Life-cycle cost-based risk assessment of aging bridge networks. *Structure and Infrastructure Engineering*, 17(4), 515-553. DOI: 10.1080/15732479.2020.1845752

[21] Han, X., & Frangopol, DM. (2023). Life-cycle risk-based optimal maintenance strategy for bridge networks subjected to corrosion and seismic hazards. *Journal of Bridge Engineering*. 28(1). DOI: 10.1061/JBENF2.BEENG-5799

[22] Abdulhadi, M., Xun'an, Zh., Fan, B., & Moman, M. (2020). Design, optimization and nonlinear response control analysis of the Mega Sub-Controlled Structural System (MSCSS) under earthquake action. *Journal of Earthquake and Tsunami*, 14(3), Article 2050013. DOI: 10.1142/S179343112050013X

[23] Huang, C., & Huang, S. (2021). Seismic resilience assessment of aging bridges with different failure modes. *Structures*, 33, 3682-3690. DOI: 10.1016/j.istruc.2021.06.066

[24] Chen, X., Guan, Z., Li, J., & Pang, Y. (2023). Repair procedure-based recovery pattern for estimating seismic resilience and novel concept of public resilience. *Disaster Prevention and Resilience*, 2(3), 16. DOI: 10.20517/dpr.2023.23

[25] Chen, X., Spencer Jr, BF., Li, J., Guan, Zh., & Pang, Y. (2022). Optimization of distribution patterns of link beams in a double-column tall pier bent subjected to earthquake excitations. *Earthquake Engineering and Structural Dynamics*, 52(3), 641-659. DOI: 10.1002/eqe.3778

[26] Chen, X., Domenico, DD., & Li, Ch. (2023). Seismic resilient design of rocking tall bridge piers using inerter-based systems. *Engineering Structures*, 281, Article 115819. DOI: 10.1016/j.engstruct.2023.115819

[27] Zhong, X., Shen, Y, Chen, X., Li, J., & Wang, Y. (2023). Seismic performance of a novel hemisphere-based rocking hinge realizing self-centering damage-free bridge system. *Engineering Structures*, 298, Article 117032. DOI: 10.1016/j.engstruct.2023.117032

[28] Omidian, P., & Khaji, N. (2022). A multi-objective optimization framework for seismic resilience enhancement of typical existing RC buildings. *Journal of Building Engineering*, 52, Article 104361. DOI: 10.1016/j.jobe.2022.104361

[29] Omidian, P., & Khaji, N. (2023). A total life-cycle cost–resilience optimization framework for infrastructures management using different retrofit strategies. *Sustainable and Resilient Infrastructure*, 1-24. DOI: 10.1080/23789689.2023.2257516

[30] Capozzo, M., Rizzi, A., Cimellaro, GP., Domaneschi, M. Barbosa, A., & Cox, D. (2019). Multi-hazard resilience assessment of a coastal community due to offshore earthquakes. *Journal of Earthquake and Tsunami*, 13(2), Article 1950008. DOI: 10.1142/S1793431119500088

[31] Cimellaro, GP., Reinhorn, AM., & Bruneau, M. (2010). Framework for analytical quantification of disaster resilience. *Engineering Structures*, 32, 3639-3649. DOI: 10.1016/j.engstruct.2010.08.008

[32] Venkittaraman, A., & Banerjee, S. (2014). Enhancing resilience of highway bridges through seismic retrofit. *Earthquake Engineering and Structural Dynamics*, 43, 1173-1191. DOI: 10.1002/eqe.2392

[33] FEMA. (2014). Multi-Hazard Loss Estimation Methodology: Earthquake Model HAZUS-MH MR5 Technical Manual, Federal Emergency Management Agency, Washington DC.

[34] Fu, Zh., Wu, D., Fang, L., Chen, D., & Ji, B. (2019). Influence factors and repair effects of seismic damage to a box section steel pier. *Journal of Earthquake and Tsunami*, 13(3-4), Article 1940001. DOI: 10.1142/S1793431119400013

[35] Fereshtehnejad, H., & Shafieezadeh, A. (2018). A multi-type multi-occurrence hazard lifecycle cost analysis framework for infrastructure management decision

making. *Engineering Structures*, 167, 504–517. DOI: 10.1016/j.engstruct.2018.04.049

[36] Padgett, JE., Nielson, BG., & DesRoches, R. (2008). Selection of optimal intensity measures in probabilistic seismic demand models of highway bridge portfolios. *Earthquake Engineering and Structural Dynamics*, 37 (5), 711–725. DOI: 10.1002/eqe.782

[37] Padgett, JE., & DesRoches, R. (2008). Methodology for the development of analytical fragility curves for retrofitted bridges. *Earthquake Engineering and Structural Dynamics*, 37 (8), 1157–1174. DOI: 10.1002/eqe.801

[38] Oregon highways seismic plus. (2014). ODOT's Oregon Highways seismic plus report, Bridge and Geo-Environmental Sections, Oregon Department of Transportation. Accessed URL:<https://www.oregon.gov/odot/Bridge/Docs_Seismic/Seismic-Plus-Report_2014.pdf>.

[39] Washington state's bridge seismic retrofit program. (2019). WSDOT's bridge seismic retrofit program and bridge resiliency assessment Data, the Washington State Department of Transportation. Accessed URL:<https://publications.anl.gov/anlpubs/2020/01/157924.pdf>.

[40] Kabir, MR., Muntasi Billah, AHM., & Shahria Alam, M. (2019). Seismic fragility assessment of a multi-span RC bridge in Bangladesh considering near-fault, far-field and long duration ground motions. *Structures*, 19, 333–348. DOI: 10.1016/j.istruc.2019.01.021

[41] Speranza, E., De Martino, G., Conte, Ch., & Dolce, M. (2023). Italian National Seismic Prevention Plan: cost analyses for risk reduction policies. *Procedia Structural Integrity*, 44, 1784-1791. DOI: 10.1016/j.prostr.2023.01.228

[42] Hwang, H., Liu, JB., & Chiu, YH. (2001). Seismic fragility analysis of highway bridges. MAEC RR-4 Project, Center for Earthquake Research and Information, The University of Memphis, TN, USA.

[43] Hedayati Dezfuli, F., & Shahria Alam, M. (2017). Effect of different steel-reinforced elastomeric isolators on the seismic fragility of a highway bridge. *Structural Control and Health Monitoring*, 24(2), Article e1866. DOI: 10.1002/stc.1866

[44] Zhang, J., & Huo, Y. (2009). Evaluating effectiveness and optimum design of isolation devices for highway bridges using the fragility function method. *Engineering Structures*, 31(8), 1648-1660. DOI: 10.1016/j.engstruct.2009.02.017

[45] Ramanathan, KN. (2012). Next generation seismic fragility curves for California bridges incorporating the evolution in seismic design philosophy. Ph.D. thesis, School of Civil and Environmental Engineering, Georgia Institute of Technology.

[46] Muntasi Billah, AHM., & Iqbal, A. (2022). Effect of seismic isolation on fragility of bridges with scoured foundations. *Journal of Structural Engineering*, 148(6), Article 04022062. DOI: 10.1061/(ASCE)ST.1943-541X.0003370

[47] Sultan, M., & Kawashima, K. (1993). Comparison of the seismic design of highway bridges in California and in Japan, Recent selected publications of Earthquake Engineering Div., Public Works Research Institute (PWRI), Japan (Technical Memorandum of PWRI No. 3276).

[48] SeismoStruct. (2023). SeismoSoft, A computer program for static and dynamic nonlinear analysis of framed structures.

[49] Fakharifar, M., Chen, G., Sneed, L., & Dalvand, A. (2015). Seismic performance of post-mainshock FRP/steel repaired RC bridge columns subjected to aftershocks. *Composites Part B: Engineering*, 72, 183-198. DOI: 10.1016/j.compositesb.2014.12.010

[50] Parghi, A., & Shahria Alam, M. (2017). Seismic collapse assessment of non-seismically designed circular RC bridge piers retrofitted with FRP composites. *Composite Structures*, 160, 901-916. DOI: 10.1016/j.compstruct.2016.10.094

[51] Mao, J., Jia, D., Yang, Z., & Xiang, N. (2020). Seismic performance of concrete bridge piers reinforced with hybrid Shape Memory Alloy (SMA) and steel bars. *Journal of Earthquake and Tsunami*, 14(1), Article 2050001. DOI: 10.1142/S1793431120500013

[52] Farrokh Ghatte, H. (2020). External steel ties and CFRP jacketing effects on seismic performance and failure mechanisms of substandard rectangular RC columns. *Composites Structures*, 248, Article 112542. DOI: 10.1016/j.compstruct.2020.112542

[53] Madas, P. (1993). Advanced Modelling of Composite Frames Subjected to Earthquake Loading, Ph.D. Thesis, Imperial College, University of London, London, UK.

[54] Mander, JB., Priestley, MJ., & Park, R. (1988). Theoretical stress-strain model for confined concrete. *Journal of Structural Engineering*, 114, 1804-1826. DOI: 10.1061/(ASCE)0733-9445(1988)114:8(1804)

[55] Martinez-Rueda, JE., & Elnashai, AS. (1997). The confined concrete model under cyclic load. *Materials and Structures*, 30, 139–147. DOI: 10.1007/BF02486385

[56] Yassin, MHN. (1994). Nonlinear analysis of prestressed concrete structures under monotonic and cyclic loads, Ph.D. Thesis, University of California, Berkeley, USA.

[57] Menegotto, M., & Pinto, PE. (1973). Method of analysis for cyclically loaded R.C. plane frames including changes in geometry and non-elastic behaviour of elements under combined normal force and bending, *Symposium on the Resistance and Ultimate Deformability of Structures Acted on by Well Defined Repeated Loads*,

International Association for Bridge and Structural Engineering, Zurich, Switzerland, pp. 15-22.

[58] Filippou, FC., Popov, EP., & Bertero, VV. (1983). Effects of bond deterioration on hysteretic behaviour of reinforced concrete joints. Report EERC 83–19, Earthquake Engineering Research Center, University of California, Berkeley.

[59] Monti, G., Nuti, C., & Santini, S. (1996). CYRUS - Cyclic Response of Upgraded Sections, Report No. 96-2, University of Chieti, Italy.

[60] Fragiadakis, M., Pinho, R., & Antoniou, S. (2008). Modelling inelastic buckling of reinforcing bars under earthquake loading, in the book: Computational Dynamics and Earthquake Engineering, 347–361. DOI: 10.1201/9780203881637.ch22

[61] Fédération International du Béton. (2006). FIB, Retrofitting of Concrete Structures by Externally Bonded FRPS, with Emphasis on Seismic Applications, FIB Bulletin No. 35, Federation Internationale du Beton, 220.

[62] Ferracuti, B., & Savoia, M. (2005). Cyclic behavior of CFRP-wrapped piers under axial and flexural loading. In Proceedings of the International Conference on Fracture, Turin, Italy.

[63] Yankelevsky, DZ., & Reinhardt, HW. (1989). Uniaxial behavior of concrete in cyclic tension. *Journal of Structural Engineering*,115(1), 166–82. DOI: 10.1061/(ASCE)0733 9445(1989)115:1(166).

[64] Yaghmaei-Sabegh, S., & Neekmanesh, Sh. (2023). Non-parametric seismic fragility curves of SDOF systems based on a clustering process. *Journal of Earthquake and Tsunami*, 17(3), Article 2350008. DOI: 10.1142/S1793431123500082

[65] Shome, N., & Cornel, CA. (1999). Probabilistic seismic demand analysis of nonlinear structures, Reliability of Marine Structures Program Technical Report RMS-35, Stanford Digital Repository.

[66] Pacific Earthquake Engineering Research Center. (2023). PEER, online strong motion database.

[69] Prakash, G. (2021). Probabilistic model for remaining fatigue life estimation of bridge components. *Journal of Structural Engineering*, 147(10). DOI: 10.1061/(ASCE)ST.1943-541X.0003114

[70] Zhao, J., Yan, Ch., Liu, Sh., Zhang, J., & Li, Sh. (2022). Hysteretic model of reinforced concrete (RC) bridge columns in saline soil environment. *Journal of Earthquake Engineering*, 26(8), 3864-3884. DOI: 10.1080/13632469.2020.1822233

[71] Biondini, F., & Vergani, M. (2015). Deteriorating beam finite element for nonlinear analysis of concrete structures under corrosion. *Structure and Infrastructure Engineering*, 11(4), 519-532. DOI: 10.1080/15732479.2014.951863

[72] Panchireddi, B., Shekhar, Sh., & Ghosh, J. (2023). Influence of ground motion duration on the seismic vulnerability of aging highway bridges. *Structure and Infrastructure Engineering*, 19(8), 1041-1063. DOI: 10.1080/15732479.2021.1998141

[73] Dizaj, EA., Madandoust, R., & Kashani, MM. (2018). Probabilistic seismic vulnerability analysis of corroded reinforced concrete frames including spatial variability of pitting corrosion. *Soil Dynamics and Earthquake Engineering*, 114, 97–112. DOI:10.1016/j.soildyn.2018.07.013

[74] Collepardi, M., Marcialis, A., & Turriziani, R. (1970). The kinetics of chloride ions penetration in concrete. *Cemento*, 67, 157-64 (In Italian).

[75] Stewart, MG., & Rosowsky, DV. (1998). Time-dependent reliability of deteriorating reinforced concrete bridge decks. *Structural Safety*, 20(1), 91–109. DOI: 10.1016/S0167-4730(97)00021-0

[76] Thoft-Christensen, P., Jensen, FM., Middleton, CR., & Blackmore, A. (1996). Assessment of the reliability of concrete slab bridges. Conf. or Workshop Item, Univ. of Cambridge, Cambridge, UK, http://publications.eng.cam.ac.uk/6361/Mar.5,2010.

[77] Ghosh, J., & Padgett, JE. (2010). Aging considerations in the development of time-dependent seismic fragility curves. *Journal of Structural Engineering*, 136(12). DOI: 10.1061/_ASCE_ST.1943-541X.0000260

[78] Xu, JG., Cai, ZK., & Feng, DC. (2021). Life-cycle seismic performance assessment of aging RC bridges considering multi-failure modes of bridge columns. *Engineering Structures,* 244, Article 112818. DOI: 10.1016/j.engstruct.2021.112818

[79] Dhakal, D. (2014). Investigation of chloride induced corrosion of bridge pier and life-cycle repair cost analysis using fiber reinforced polymer composites. M.Sc. thesis, Department of Civil and Environmental Engineering and Construction, University of Nevada, Las Vegas, UNLV University Libraries. DOI: 10.34917/7048176

[80] Liang, H., Li, Sh., Lu, Y., Hu, J., & Liu, Zh. (2019). Electrochemical performance of corroded reinforced concrete columns strengthened with fiber reinforced polymer. *Composite Structures,* 2.7, 576-588. DOI: 10.1016/j.compstruct.2018.09.028

[81] Khawaja, MA., Sen, R., & Bhethanabotla, V. (2020). Predictive framework for FRP-concrete corrosion repair. *Journal of Composites for Construction,* 24(6). DOI: 10.1061/(ASCE)CC.1943-5614.0001082

[82] Gopu, GN., & Joseph, SA. (2022). Corrosion behavior of fiber-reinforced concrete-A Review. *Fibers,* 10(5). DOI: 10.3390/fib10050038

[83] El Maaddawy, T., Chahrour, A., & Soudki, K. (2006). Effect of Fiber-Reinforced Polymer Wraps on Corrosion Activity and Concrete Cracking in Chloride-Contaminated Concrete Cylinders. *Journal of Composites for Construction*, 10(2), 139–147. DOI: 10.1061/(ASCE)1090-0268(2006)10:2(139)

[84] Monila, FJ., Alonso, C., & Andrade, C. (1993). Cover cracking as a function of rebar corrosion: Part 2—Numerical model. *Materials and Structures*, 26(9), 532-548. DOI: 10.1007/BF02472864

[85] Panchireddi, B., & Ghosh, J. (2021). Probabilistic seismic loss estimation of aging highway bridges subjected to multiple earthquake events. *Structure and Infrastructure Engineering,* 17(9), 115-117. DOI: 10.1080/15732479.2020.1801765

[86] Du, YG., Clark, LA., & Chan, AHC. (2005). Residual capacity of corroded reinforcing bars. *Magazine of Concrete Research,* 57(3), 135-147. DOI: 10.1680/macr.2005.57.3.135

[87] Andisheh, K., Scott, A., & Palermo, A. (2016). Seismic behaviour of corroded RC bridges: Review and research gaps. *International Journal of Corrosion,* Article 3075184. DOI: 10.1155/2016/3075184

[88] Apostolopoulos, CA., & Papadakis, VG. (2008). Consequences of steel corrosion on the ductility properties of reinforcement bar. *Construction and Building Materials,* 22(12), 2316-2324. DOI: 10.1016/j.conbuildmat.2007.10.006

[89] American Association of State Highway and Transportation Officials (2014). AASHTO, LRFD bridge design specifications (7th ed.). Washington, DC: American Association of State Highway and Transportation Officials.

[90] Omidian, P., & Saffari, H. (2018). Comparative analysis of seismic behavior of RC buildings with shape memory alloy rebar in regular, torsional irregularity and extreme torsional irregularity cases. *Journal of Building Engineering*, 20, 723–753. DOI: 10.1016/j.jobe.2018.09.020

[91] Bianchi, F., Sousa, R., Pinho, R. (2011). Blind prediction of a full-scale RC bridge column tested under dynamic conditions, Proceedings of 3rd International Conference on Computational Methods in Structural Dynamics and Earthquake Engineering, COMPDYN 2011, Paper no. 294, Corfu, Greece.

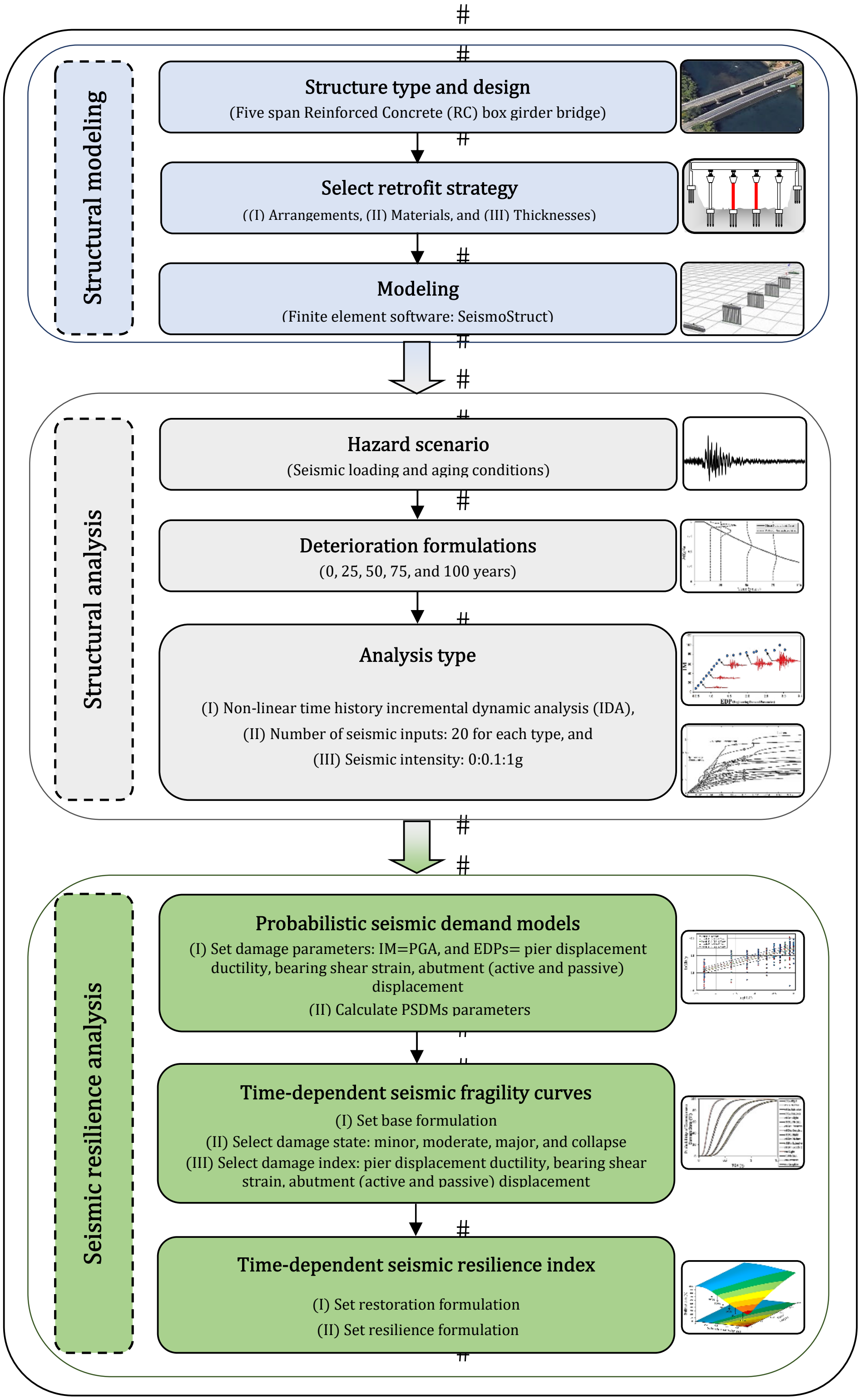

Fig. 1. The flowchart of the time-dependent seismic resilience assessment process of this study.

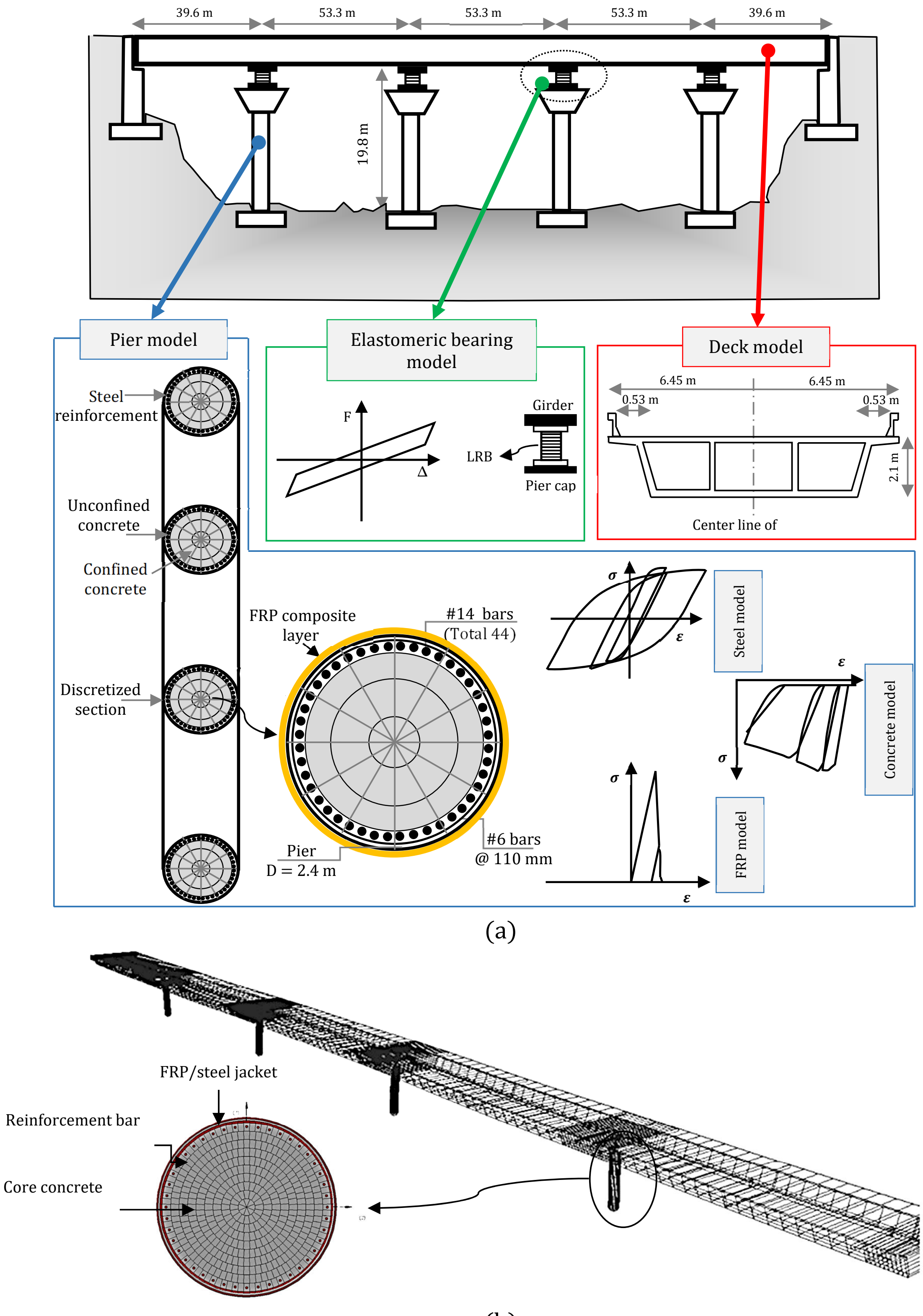

Fig. 2. Typical details of (a) the bridge under investigation and (b) finite element model specifications of the considered bridge in SeismoStruct software.

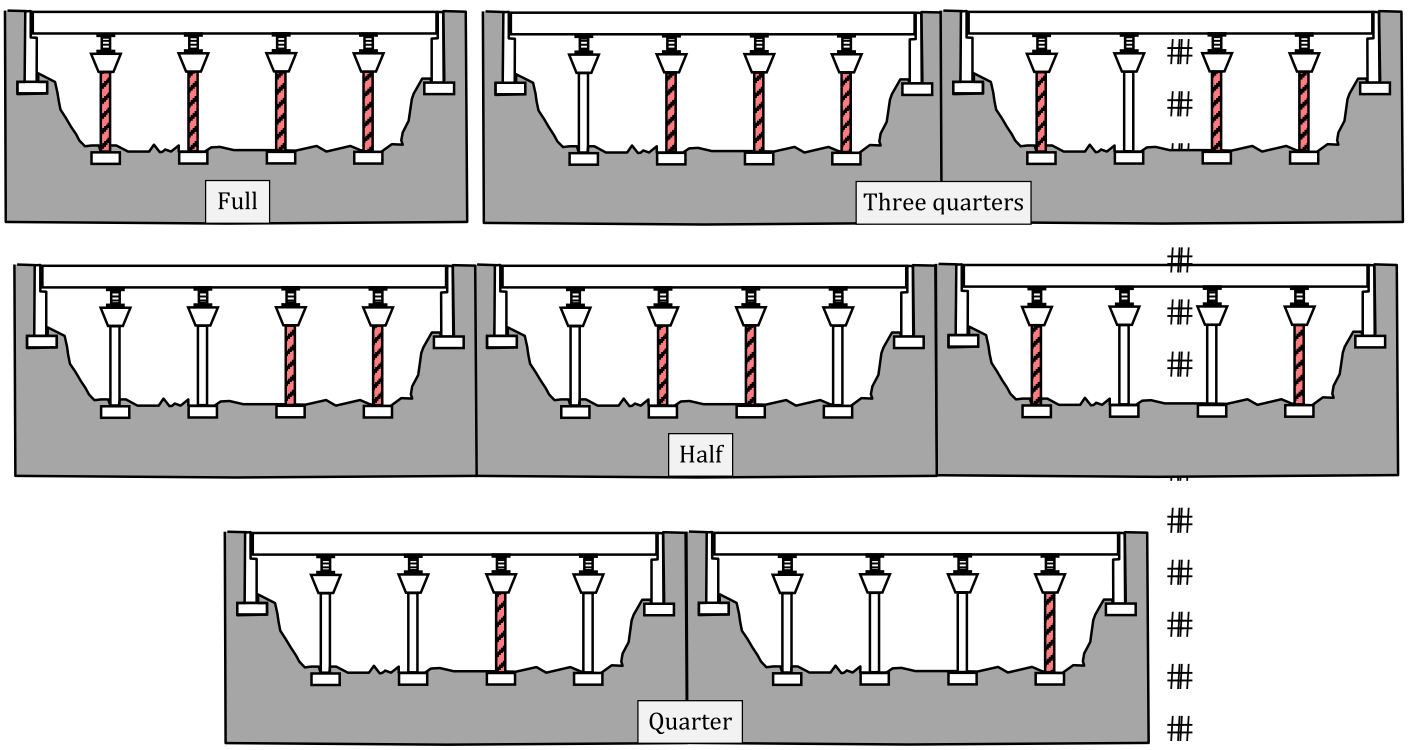

Fig. 3. Various arrangements used for bridge pier retrofitting configurations.

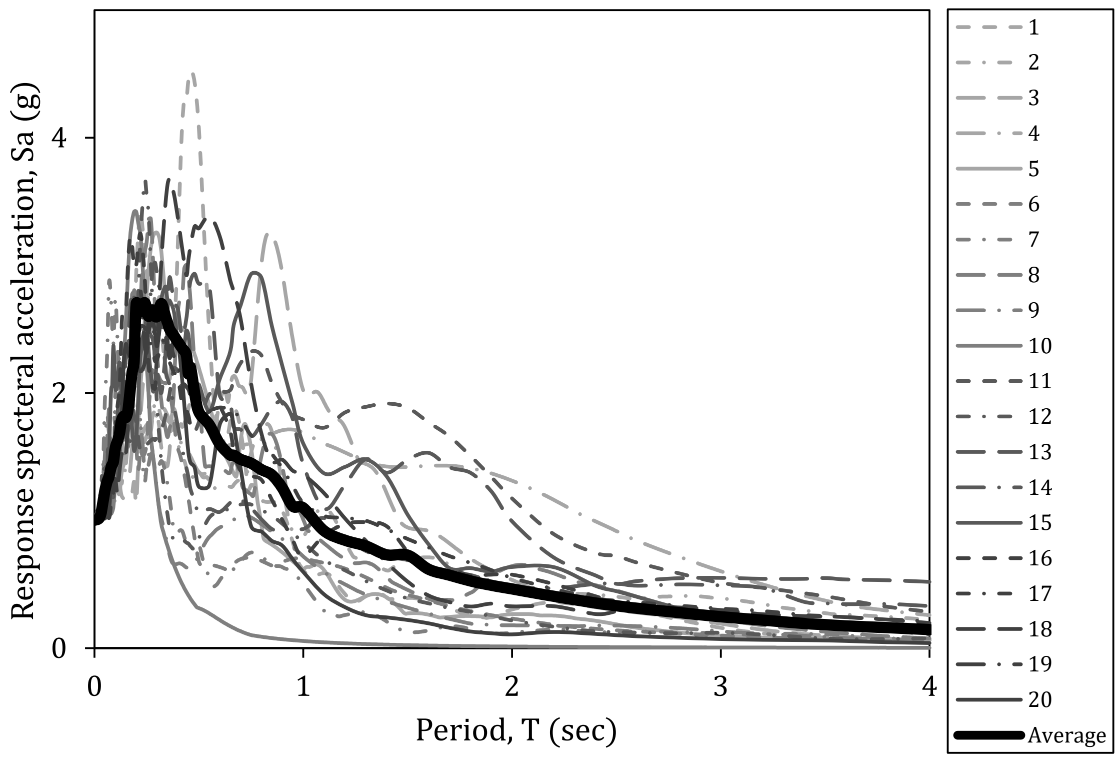

Fig. 4. Scaled acceleration response spectrum of selected earthquake records used in this study.

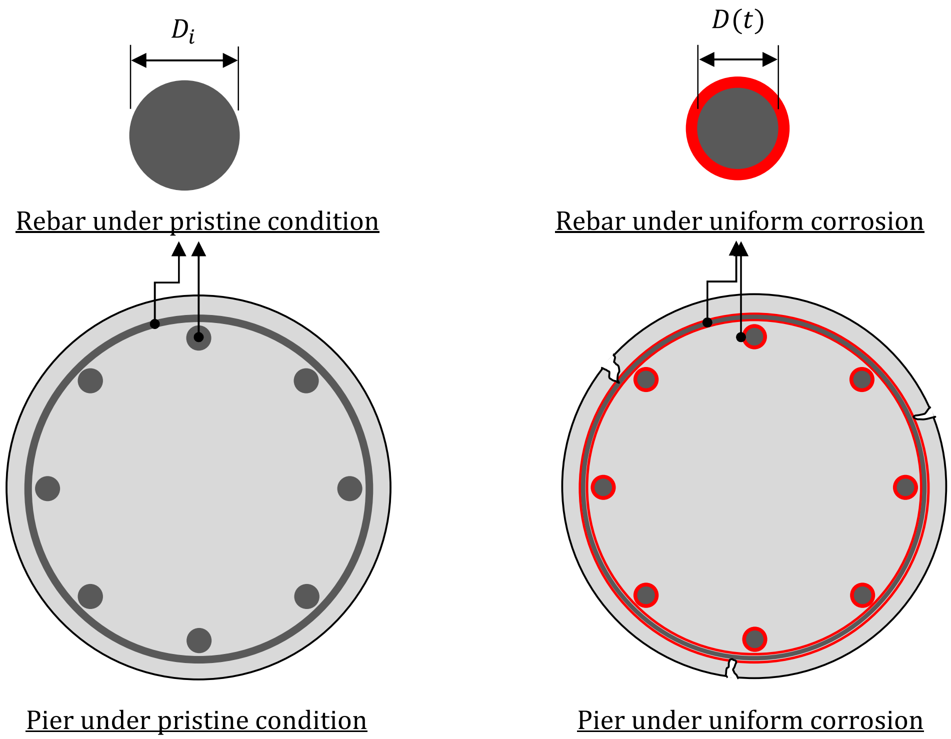

D_i
$D(t)$
Rebar under pristine condition
Rebar under uniform corrosion
Pier under pristine condition
Pier under uniform corrosion

(a)

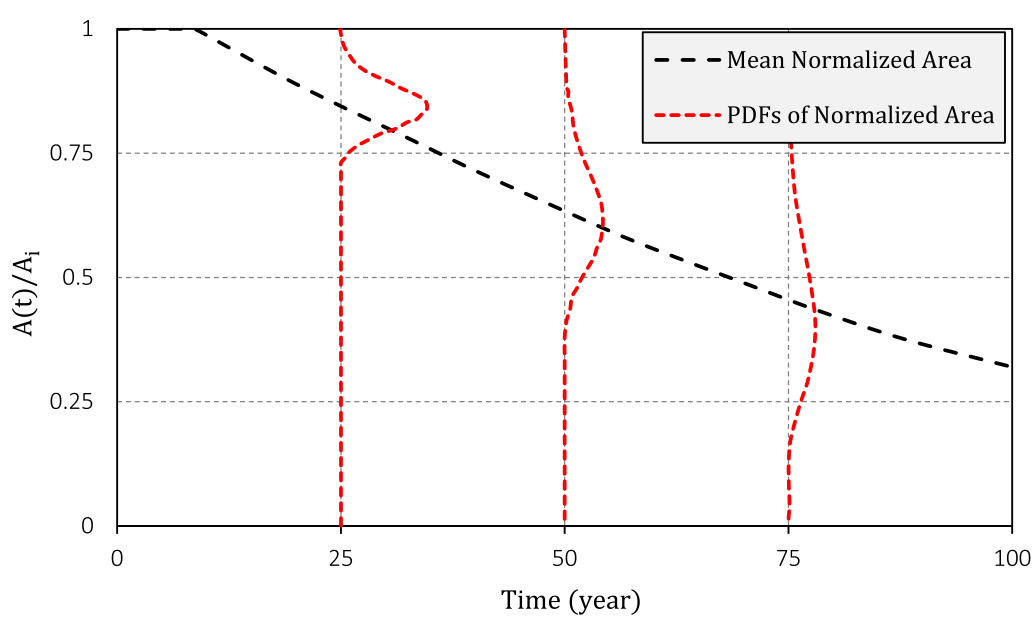

Mean Normalized Area
PDFs of Normalized Area
$A(t)/A_i$
1
0.75
0.5
0.25
0
0
25
50
75
100
Time (year)

(b)

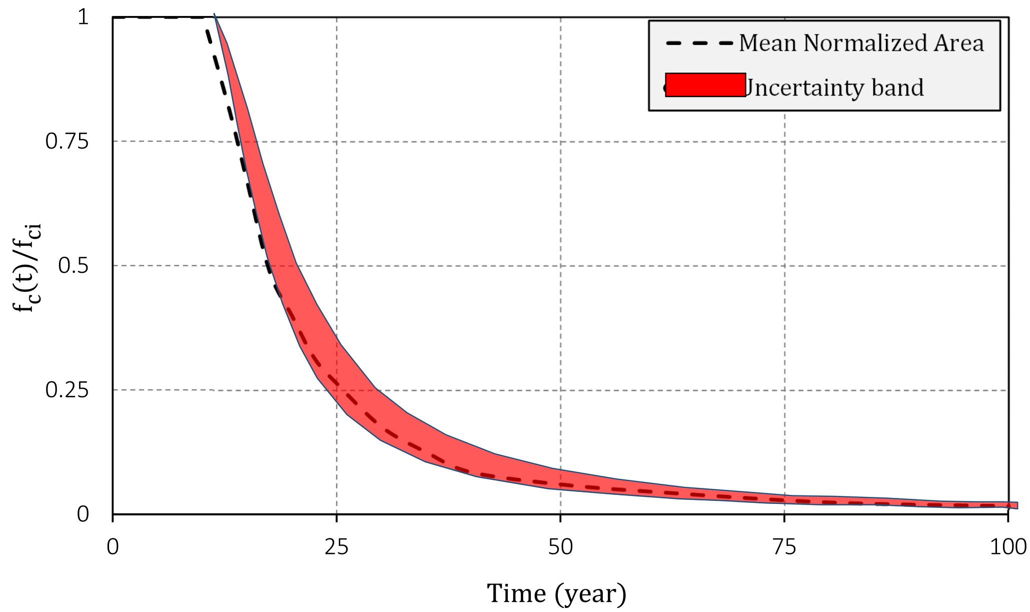

(c)

Fig. 5. Modeling of RC piers depends on the time during the service life for (a) schematic cross-section reduction of a uniform corroded reinforcing steel bar, (b) distribution of normalized time-variant area reduction of the reinforcing steel area, and (c) mean cover concrete strength with time along with the lower and upper limits of the uncertainty band representing 5th and 95th percentile confidence bounds.

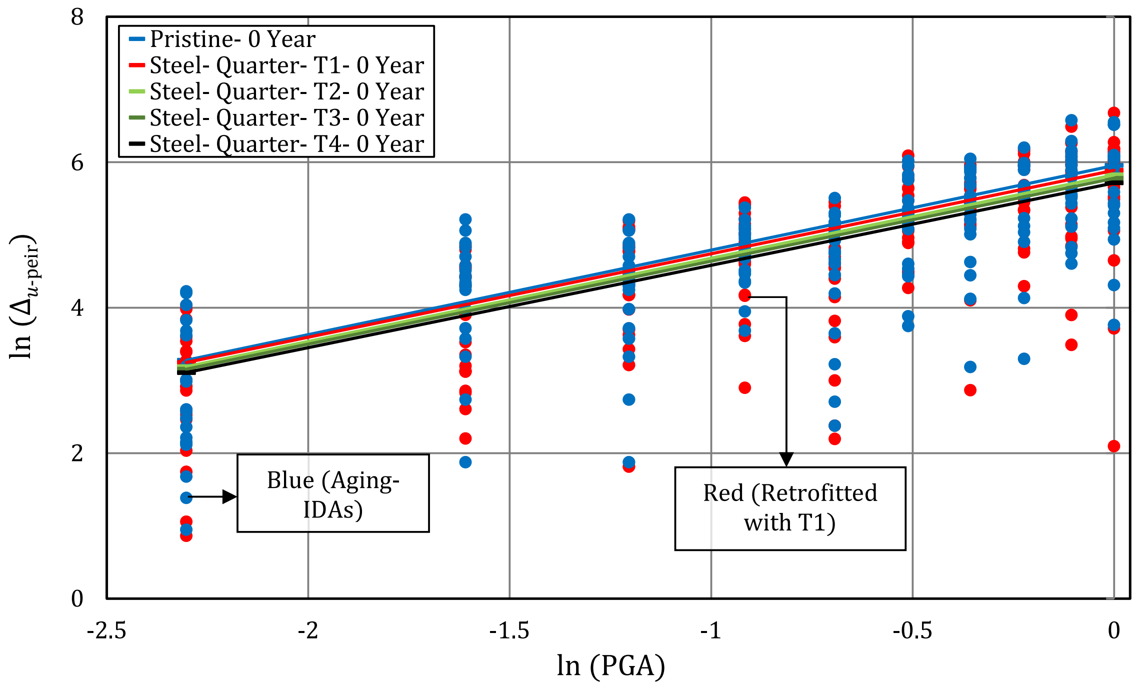
Pristine- 0 Year
Steel- Quarter- T1- 0 Year
Steel- Quarter- T2- 0 Year
Steel- Quarter- T3- 0 Year
Steel- Quarter- T4- 0 Year
Blue (Aging-IDAs)
Red (Retrofitted with T1)
ln ($\Delta_{u\text{-peir}}$)
ln (PGA)
0
2
4
6
8
-2.5
-2
-1.5
-1
-0.5
0
(a)

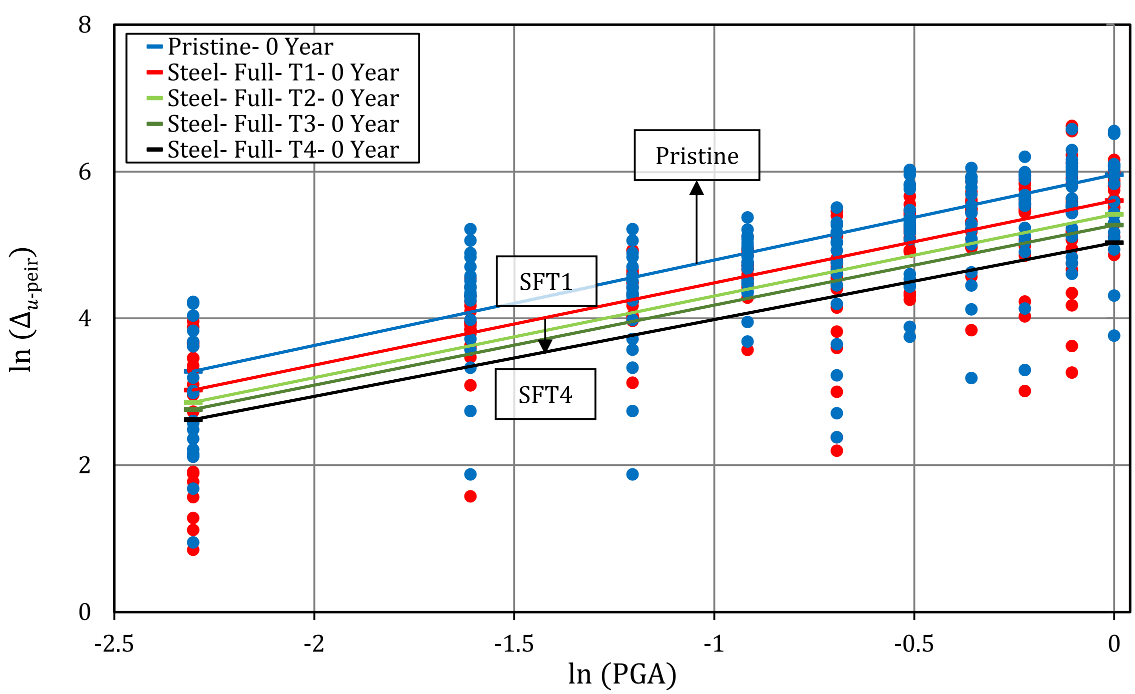
Pristine- 0 Year
Steel- Full- T1- 0 Year
Steel- Full- T2- 0 Year
Steel- Full- T3- 0 Year
Steel- Full- T4- 0 Year
Pristine
SFT1
SFT4
ln ($\Delta_{u\text{-peir}}$)
ln (PGA)
0
2
4
6
8
-2.5
-2
-1.5
-1
-0.5
0
(b)#

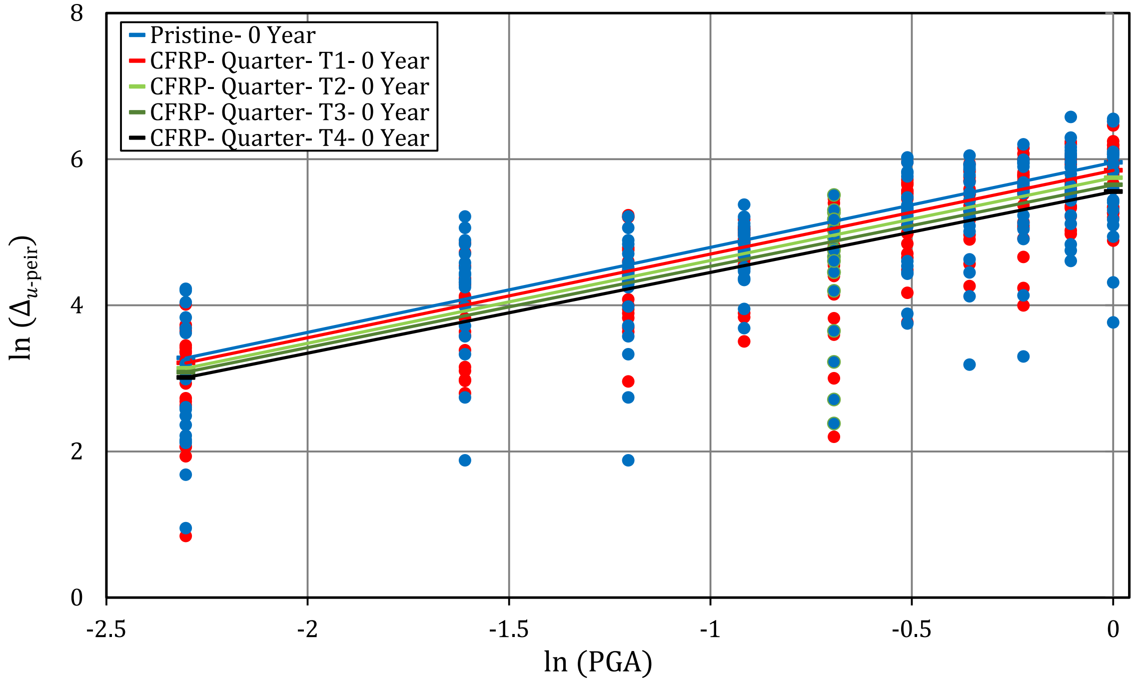

(c)

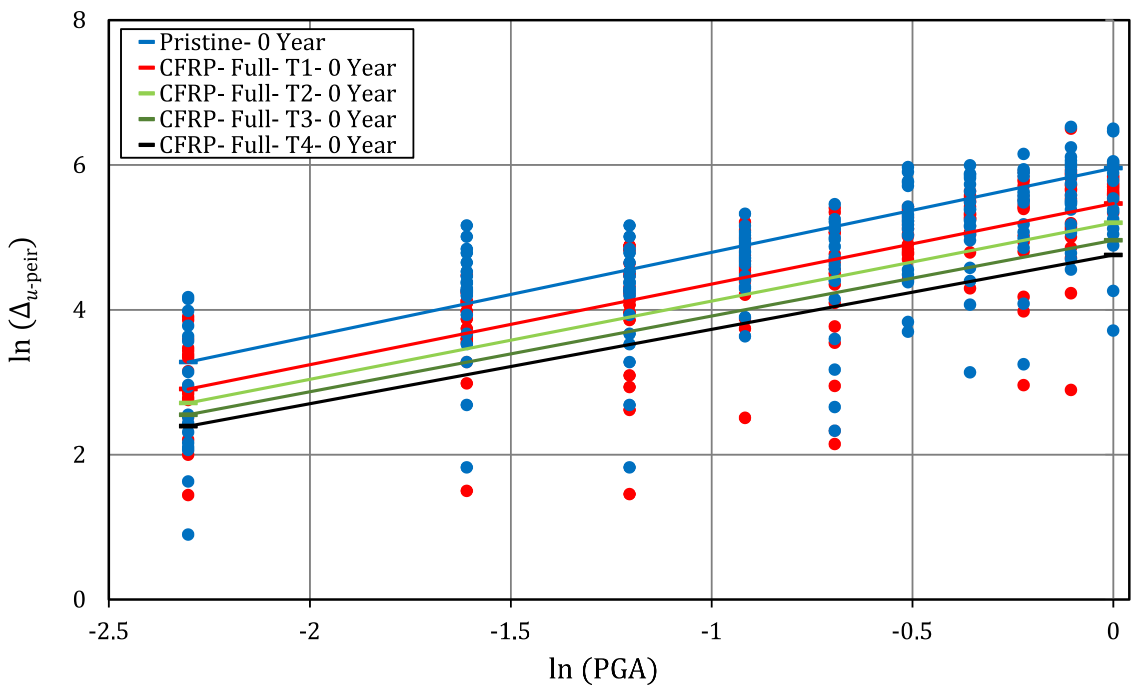

(d)

Fig. 6. IDAs results and fitted PSDMs of bridge piers for (a) Quarter-steel jacketing, (b) Full-steel jacketing, (c) Quarter-CFRP jacketing, and (d) Full-CFRP jacketing at pristine state (0 year aging).

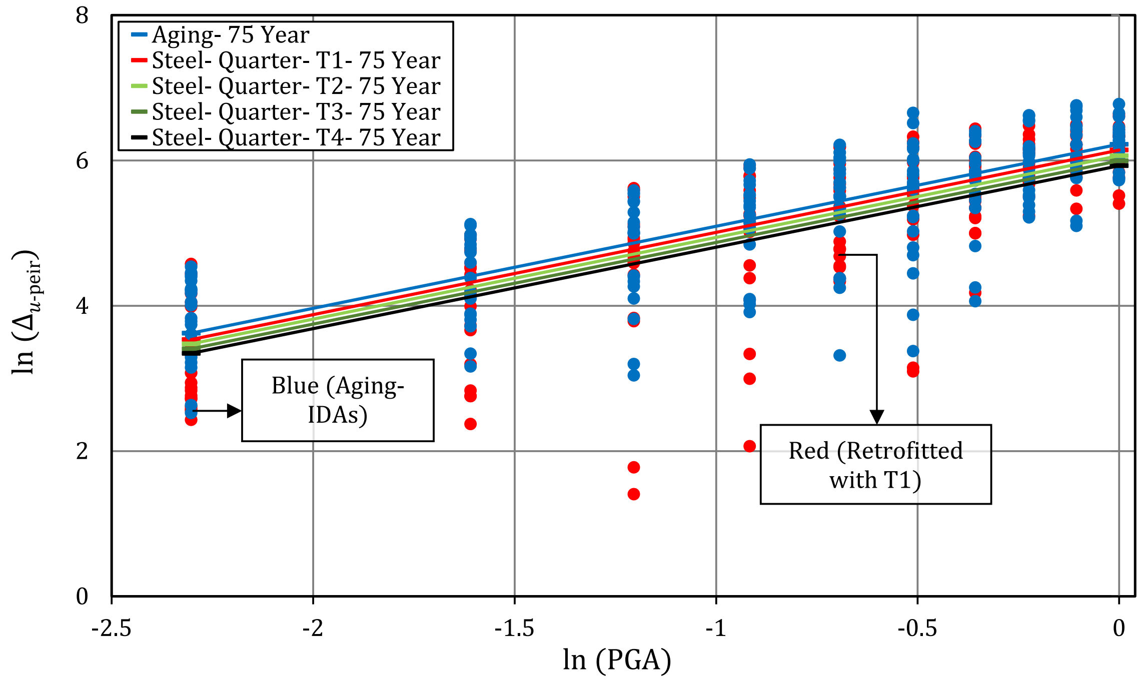
Aging- 75 Year
Steel- Quarter- T1- 75 Year
Steel- Quarter- T2- 75 Year
Steel- Quarter- T3- 75 Year
Steel- Quarter- T4- 75 Year
Blue (Aging- IDAs)
Red (Retrofitted with T1)
ln ($\Delta_{u\text{-peir}}$)
ln (PGA)

(a)

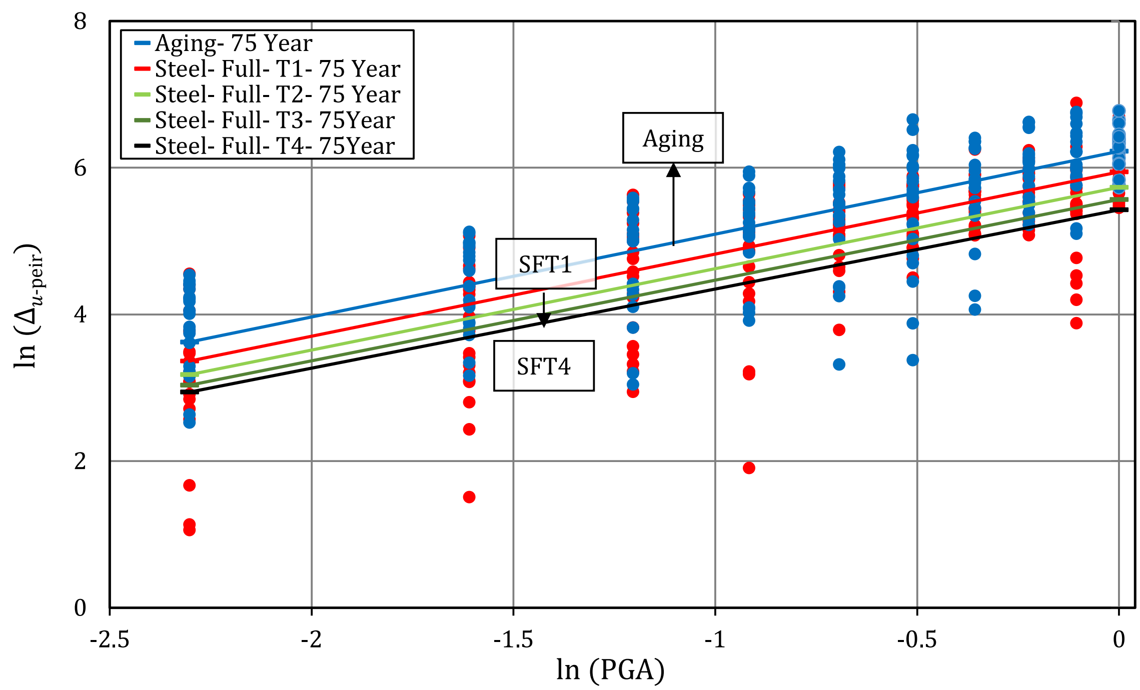
Aging- 75 Year
Steel- Full- T1- 75 Year
Steel- Full- T2- 75 Year
Steel- Full- T3- 75Year
Steel- Full- T4- 75Year
Aging
SFT1
SFT4
ln ($\Delta_{u\text{-peir}}$)
ln (PGA)

(b)#

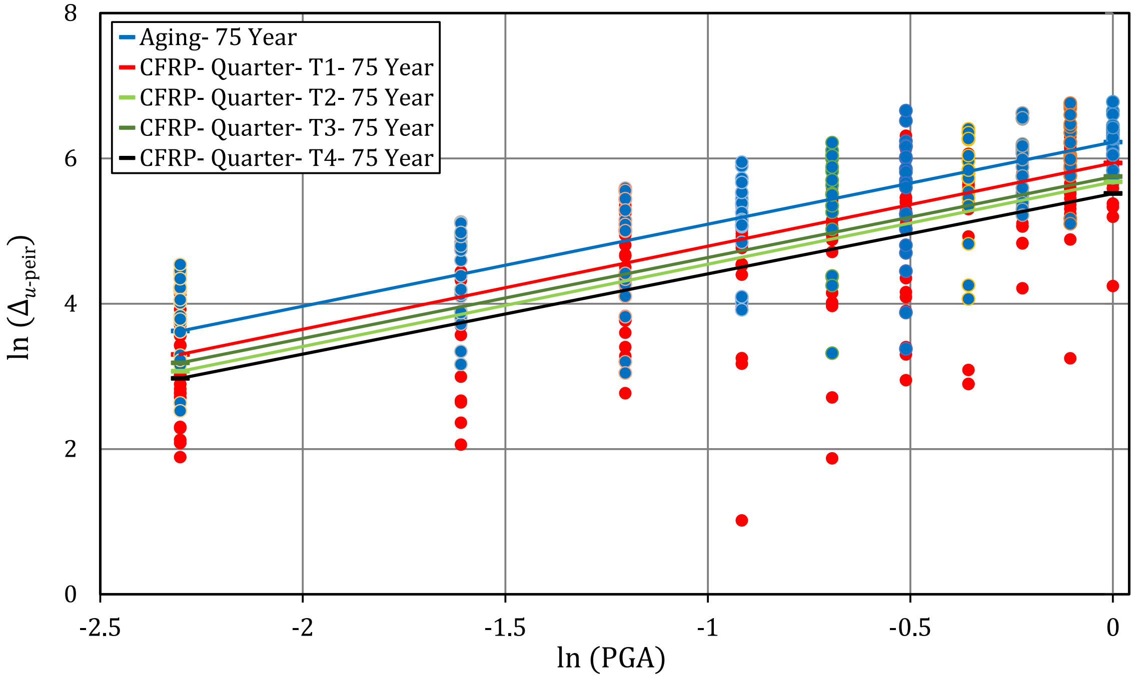

(c)

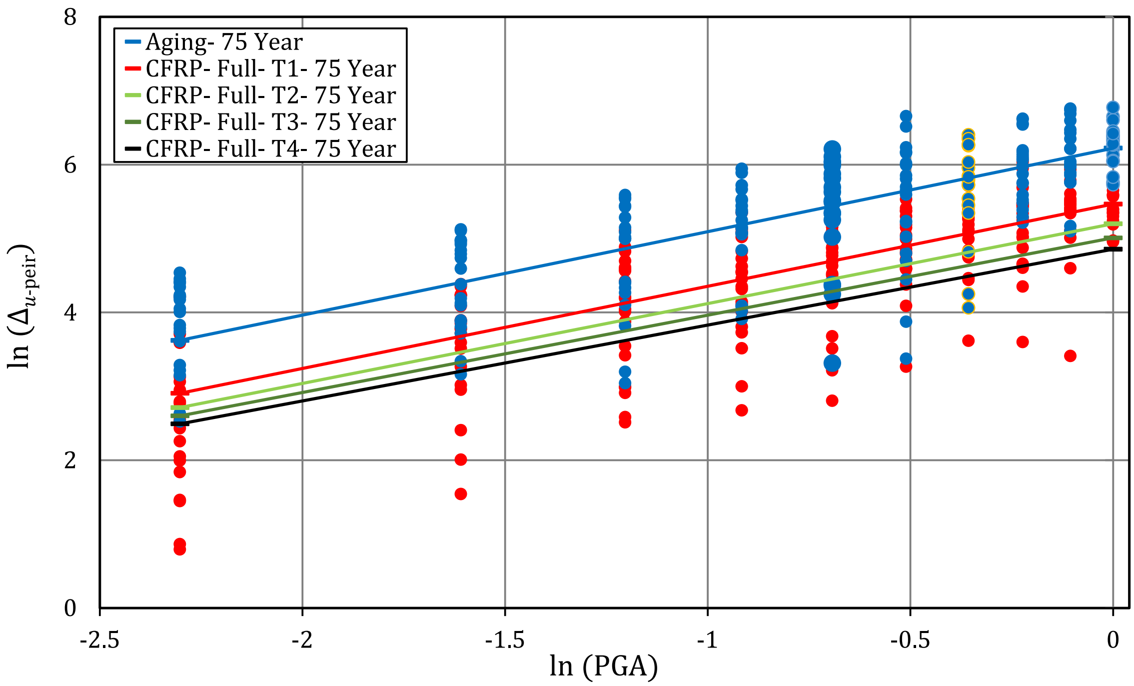

(d)

Fig. 7. IDAs results and fitted PSDMs of bridge piers for (a) Quarter-steel jacketing, (b) Full-steel jacketing, (c) Quarter-CFRP jacketing, and (d) Full-CFRP jacketing when they were exposed to chloride-induced corrosion at 75 years of service life.

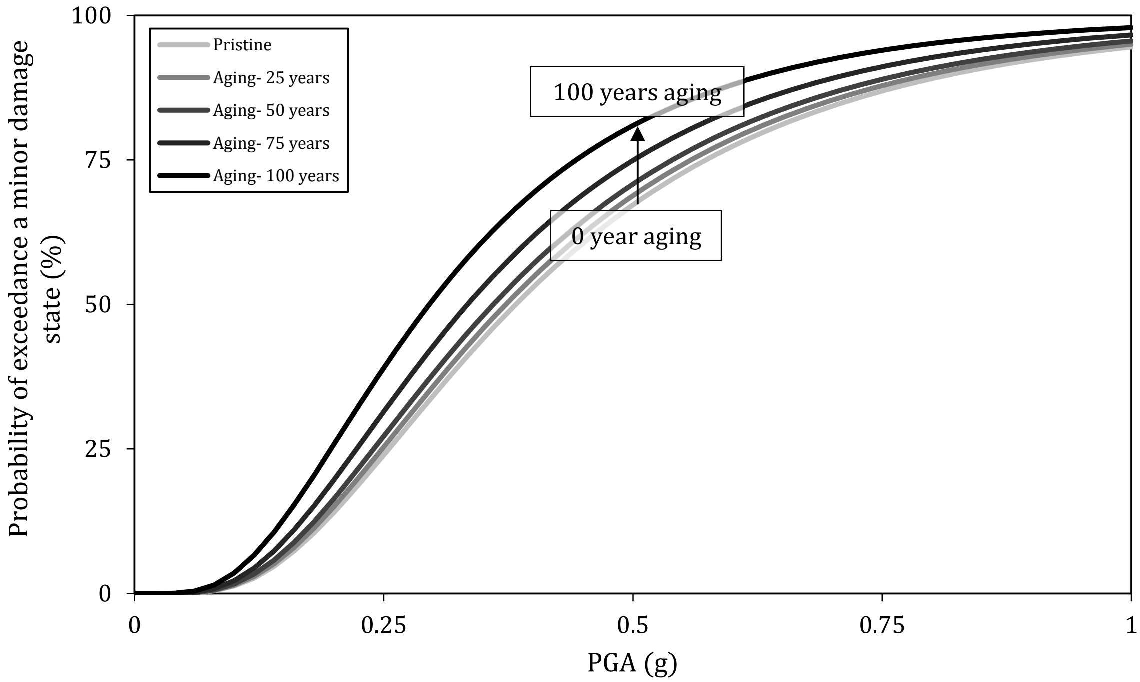

Pristine
Aging- 25 years
Aging- 50 years
Aging- 75 years
Aging- 100 years
100 years aging
0 year aging
Probability of exceedance a minor damage state (%)
PGA (g)
0
25
50
75
100
0.25
0.5
0.75
1

(a)

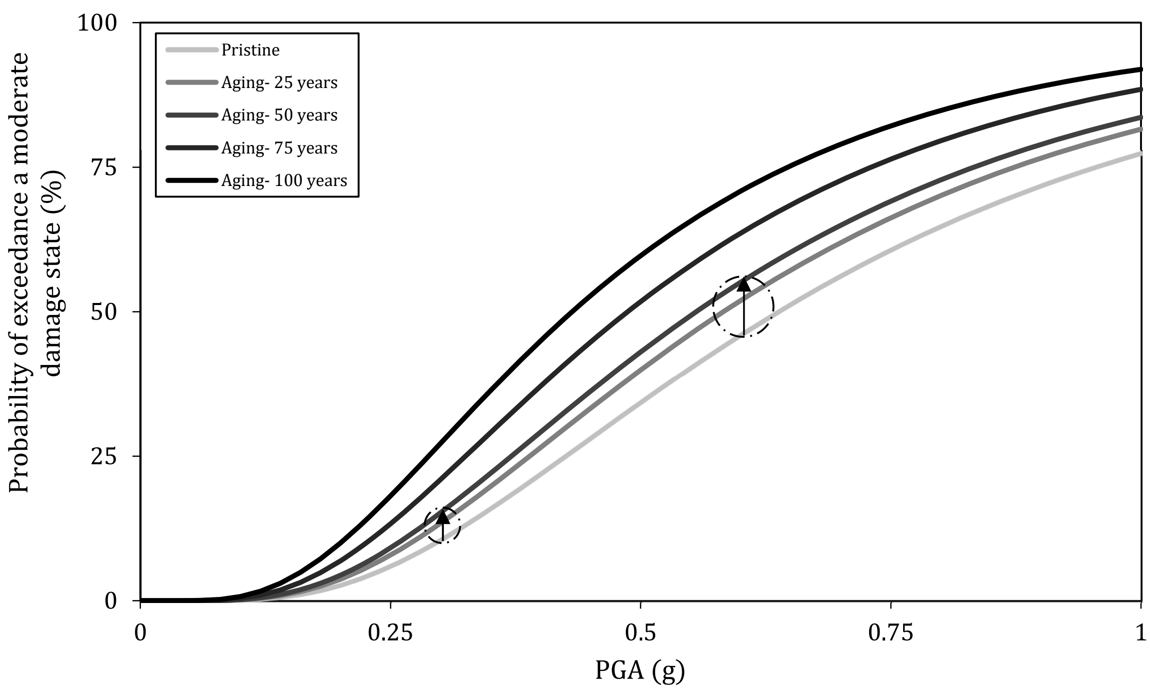

Pristine
Aging- 25 years
Aging- 50 years
Aging- 75 years
Aging- 100 years
Probability of exceedance a moderate damage state (%)
PGA (g)
0
25
50
75
100
0.25
0.5
0.75
1

(b)#

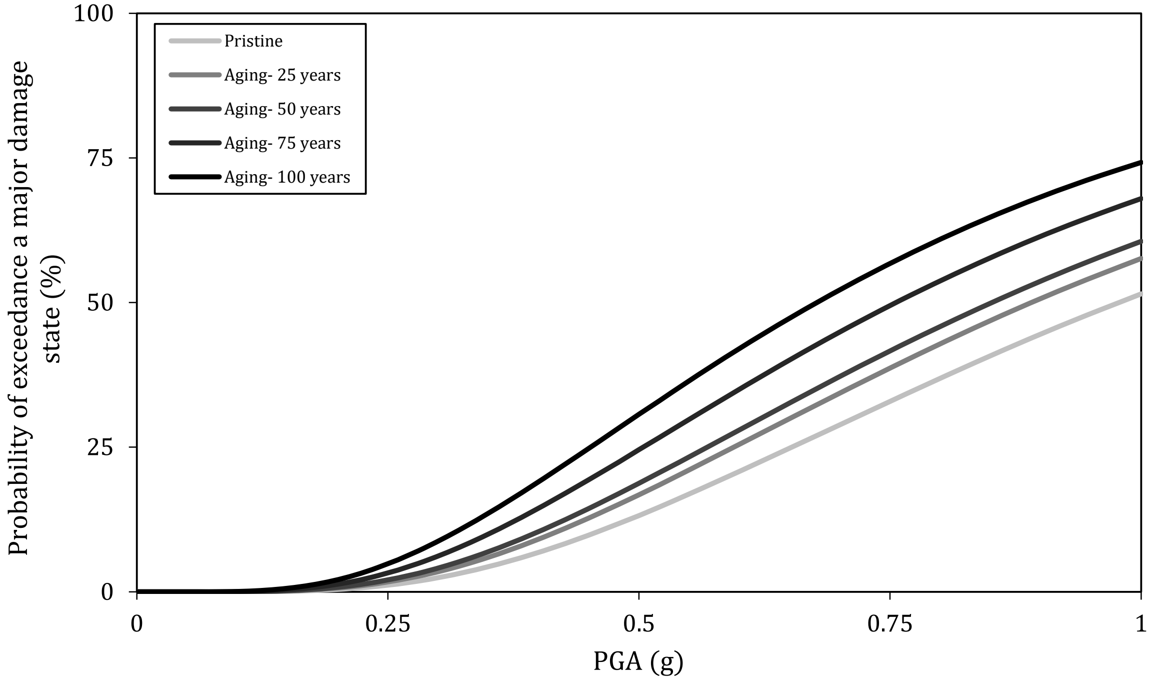

(c)

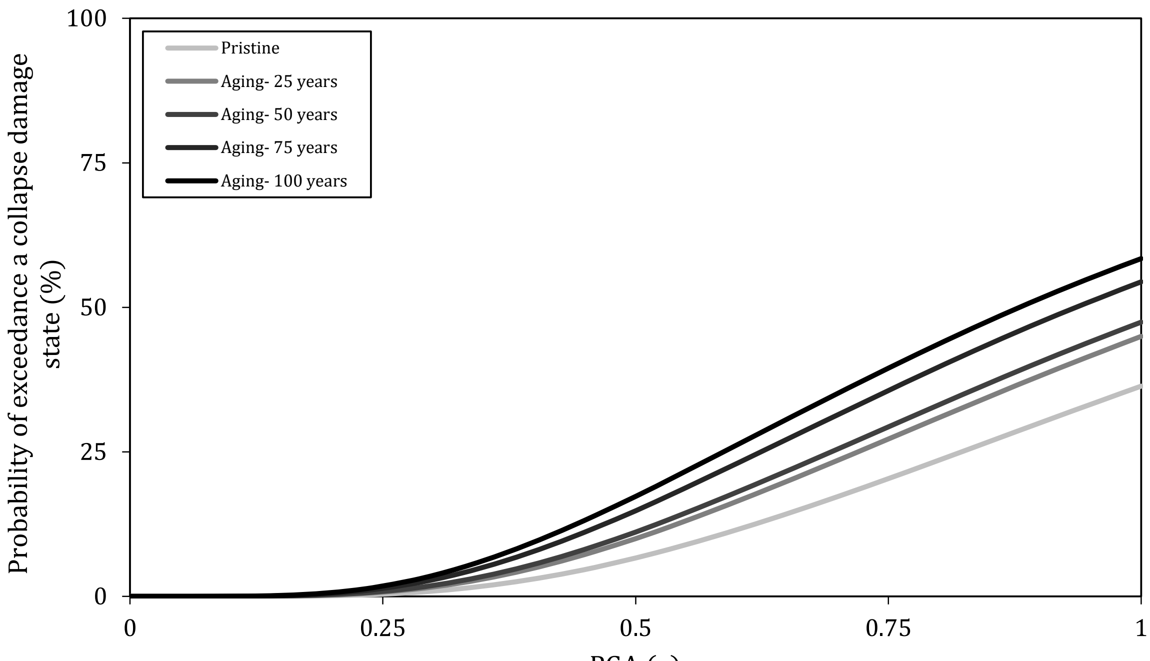

(d)

Fig. 8. Seismic fragility curves of non-retrofitted bridge system for (a) minor, (b) moderate, (c) major, and (d) collapse damage states along its life-cycle.

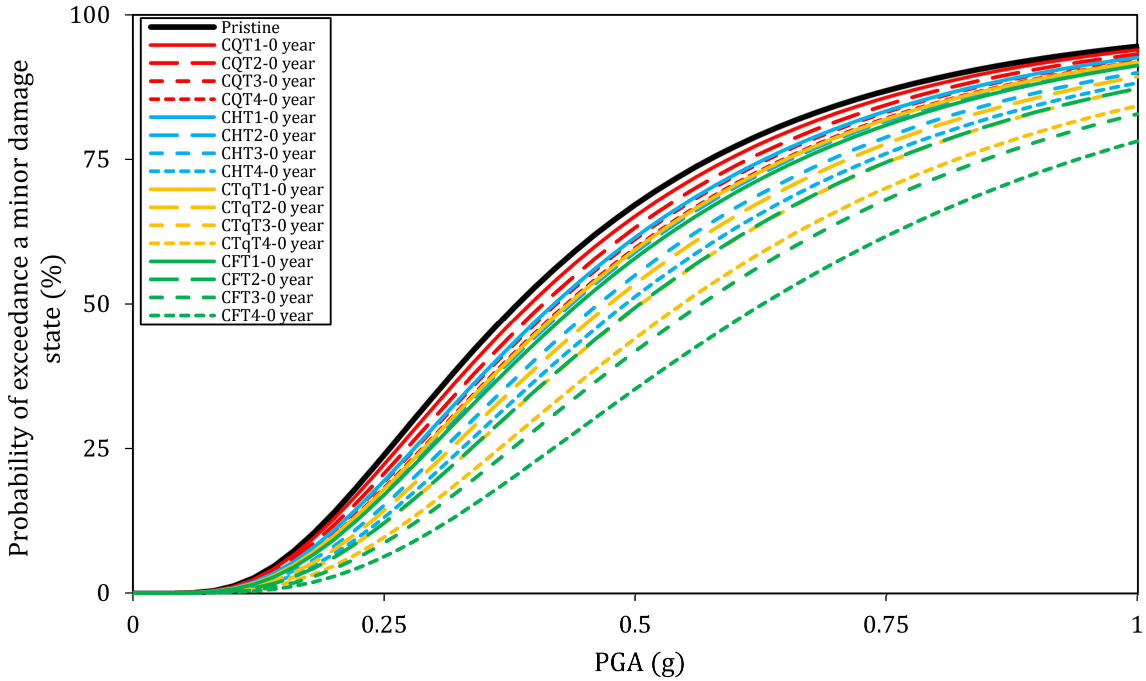

Pristine
CQT1-0 year
CQT2-0 year
CQT3-0 year
CQT4-0 year
CHT1-0 year
CHT2-0 year
CHT3-0 year
CHT4-0 year
CTqT1-0 year
CTqT2-0 year
CTqT3-0 year
CTqT4-0 year
CFT1-0 year
CFT2-0 year
CFT3-0 year
CFT4-0 year
Probability of exceedance a minor damage state (%)
PGA (g)

(a)

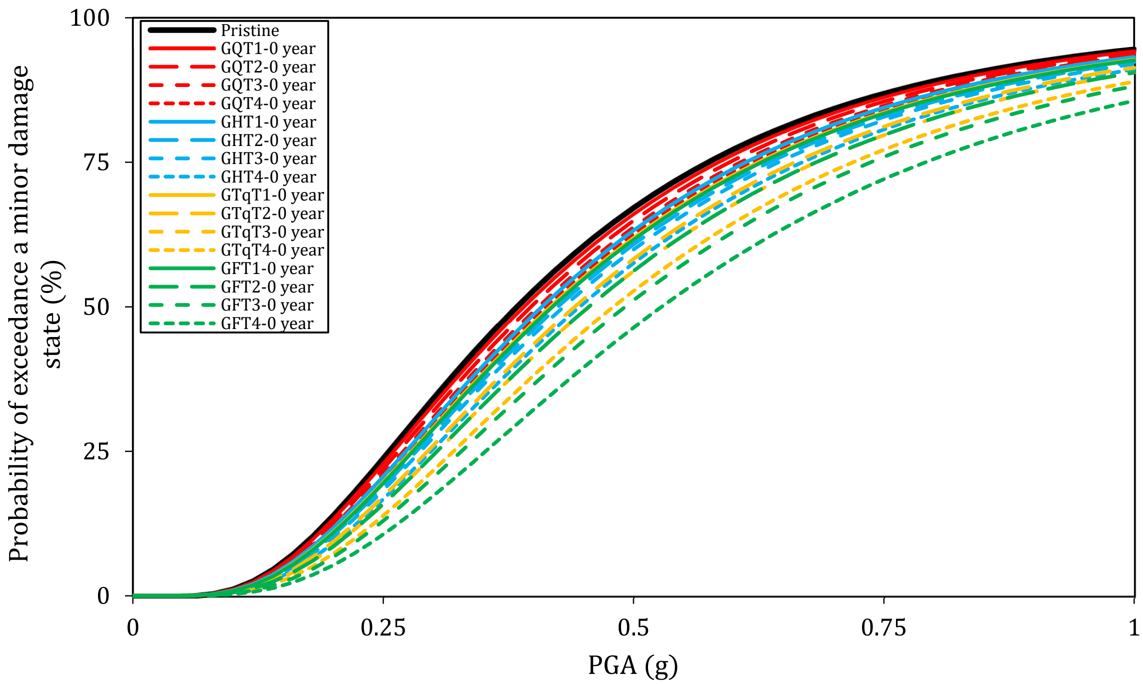

Pristine
GQT1-0 year
GQT2-0 year
GQT3-0 year
GQT4-0 year
GHT1-0 year
GHT2-0 year
GHT3-0 year
GHT4-0 year
GTqT1-0 year
GTqT2-0 year
GTqT3-0 year
GTqT4-0 year
GFT1-0 year
GFT2-0 year
GFT3-0 year
GFT4-0 year
Probability of exceedance a minor damage state (%)
PGA (g)

(b)#

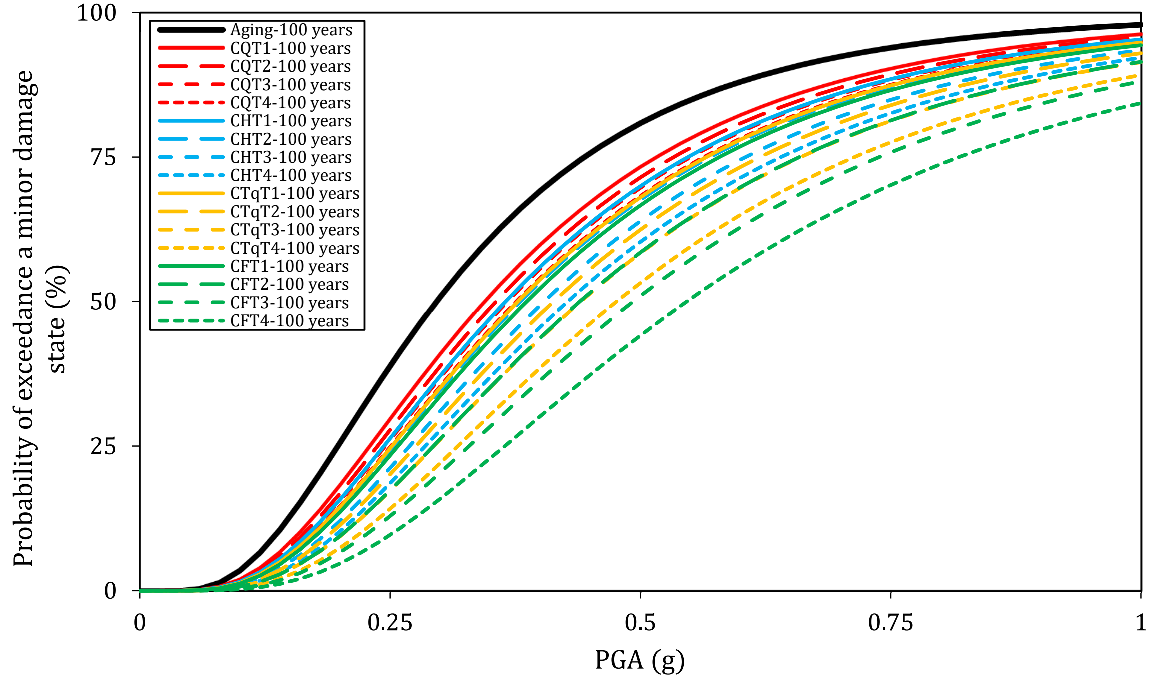

(c)

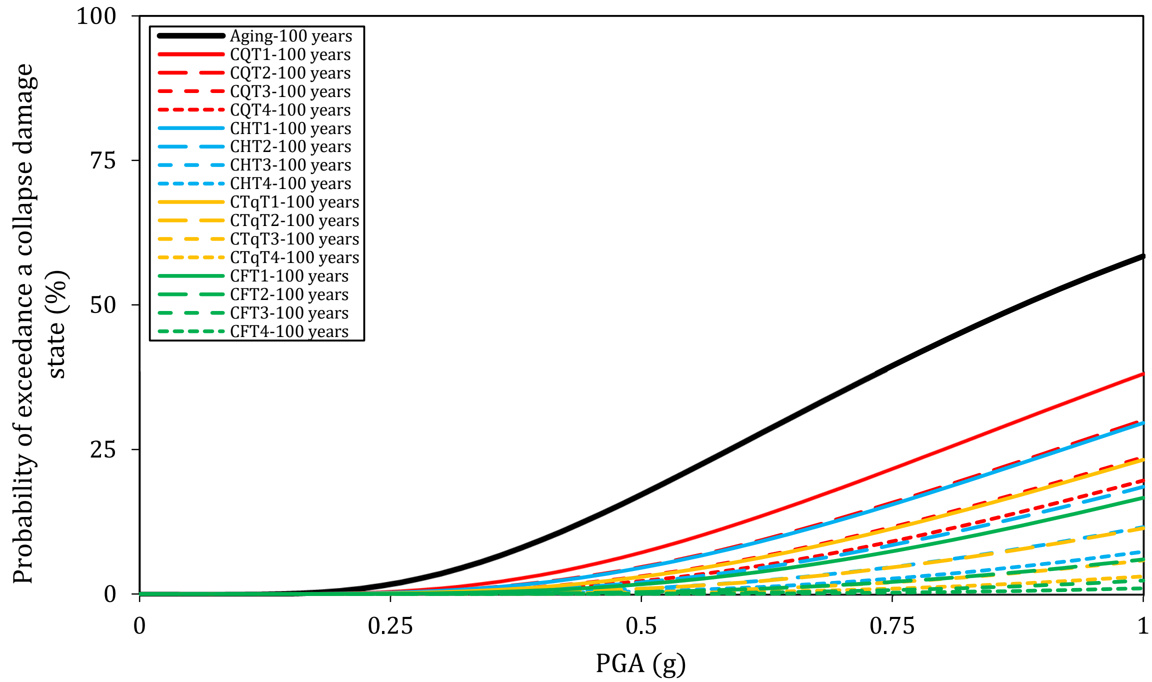

(d)

Fig. 9. Seismic fragility curves for (a) CFRP and (b) GFRP jacketings at minor damage state, with 0 year of aging. Seismic fragility curves for CFRP jacketings at (c) minor and (d) collapse damage states with 100 years of aging under corrosion.

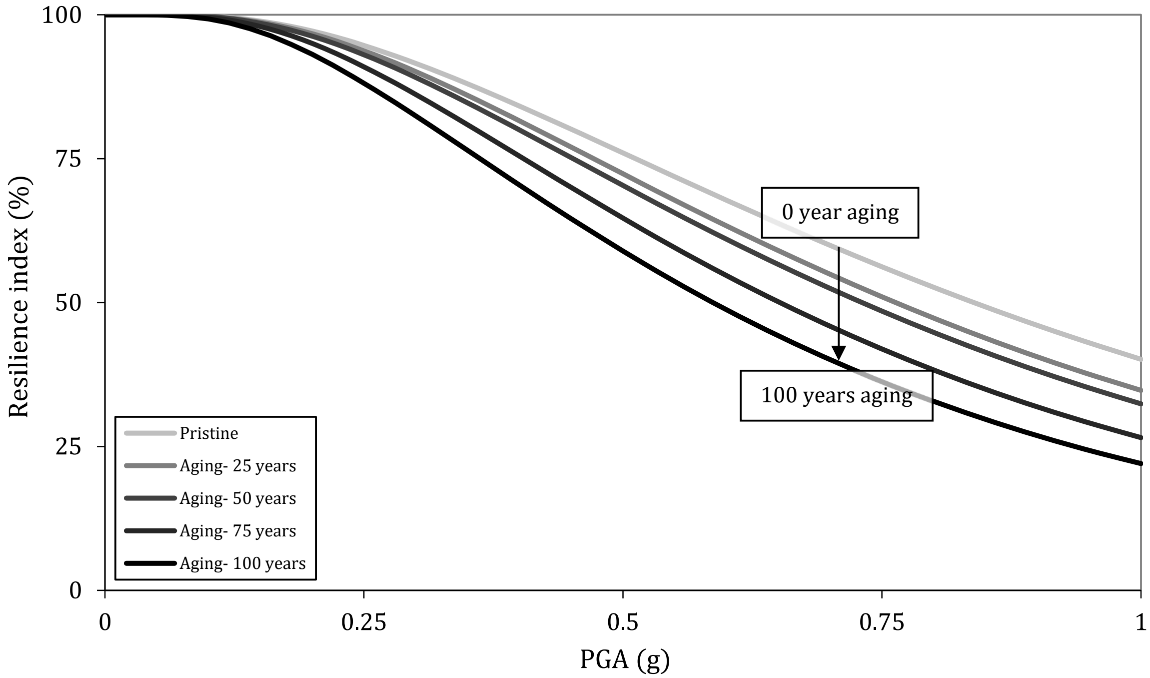

100
75
50
25
0
0
0.25
0.5
0.75
1
Resilience index (%)
PGA (g)
0 year aging
100 years aging
Pristine
Aging- 25 years
Aging- 50 years
Aging- 75 years
Aging- 100 years

(a)

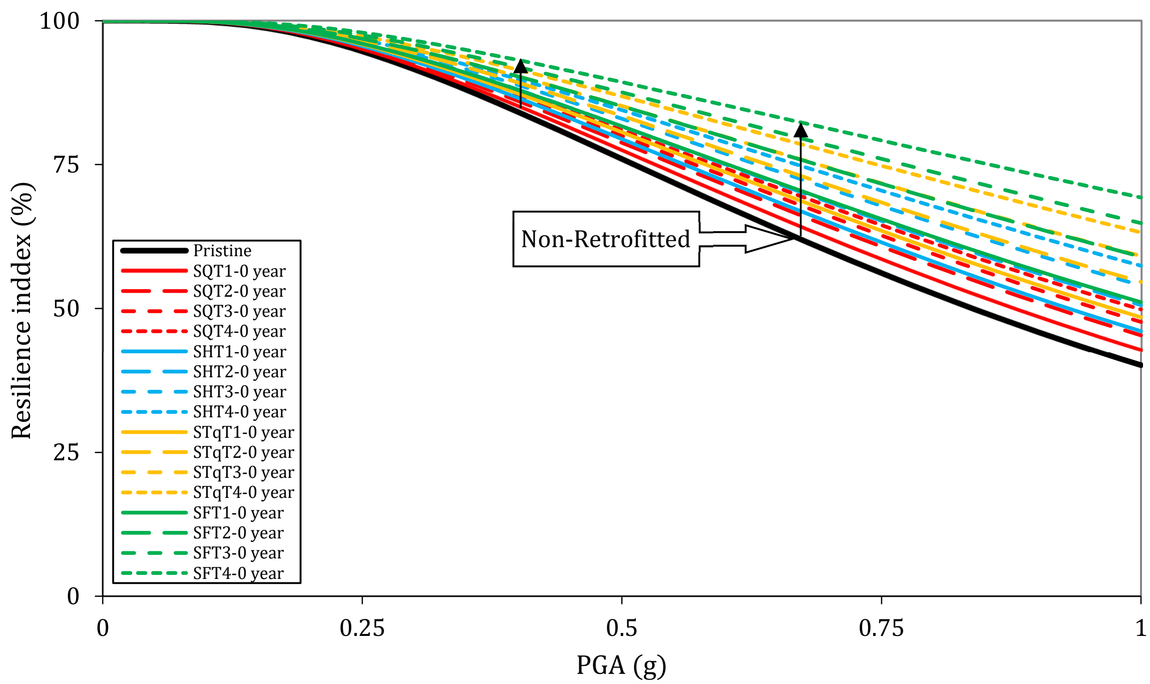

100
75
50
25
0
0
0.25
0.5
0.75
1
Resilience inddex (%)
PGA (g)
Non-Retrofitted
Pristine
SQT1-0 year
SQT2-0 year
SQT3-0 year
SQT4-0 year
SHT1-0 year
SHT2-0 year
SHT3-0 year
SHT4-0 year
STqT1-0 year
STqT2-0 year
STqT3-0 year
STqT4-0 year
SFT1-0 year
SFT2-0 year
SFT3-0 year
SFT4-0 year

(b)

#

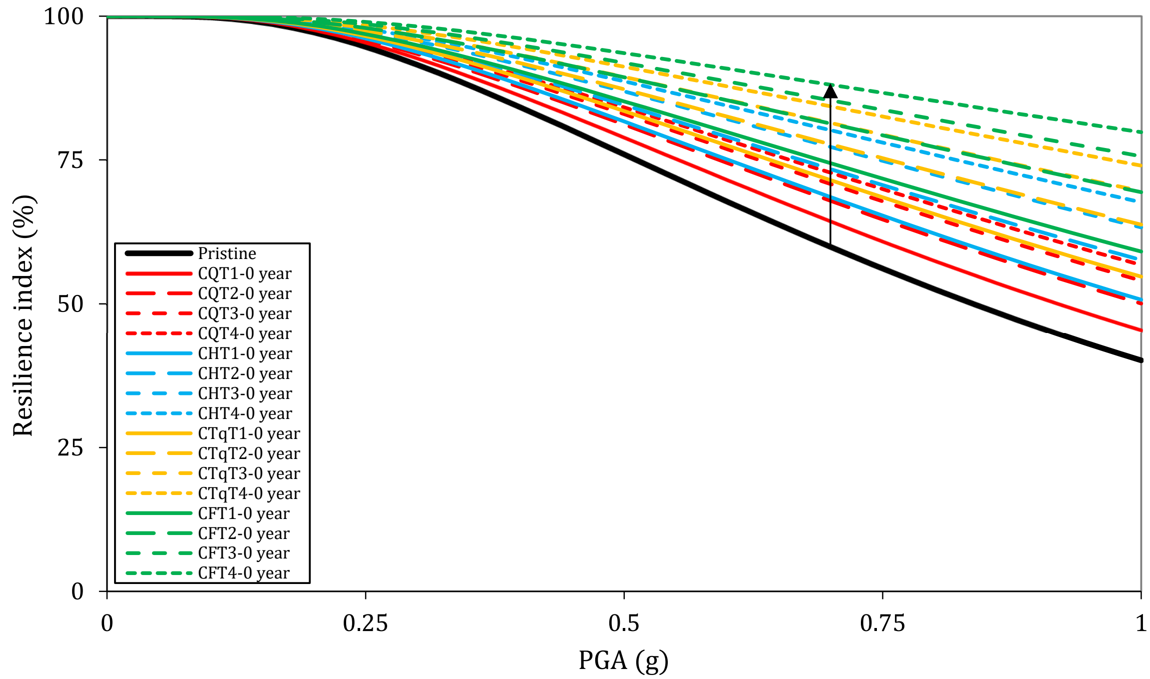

(c)

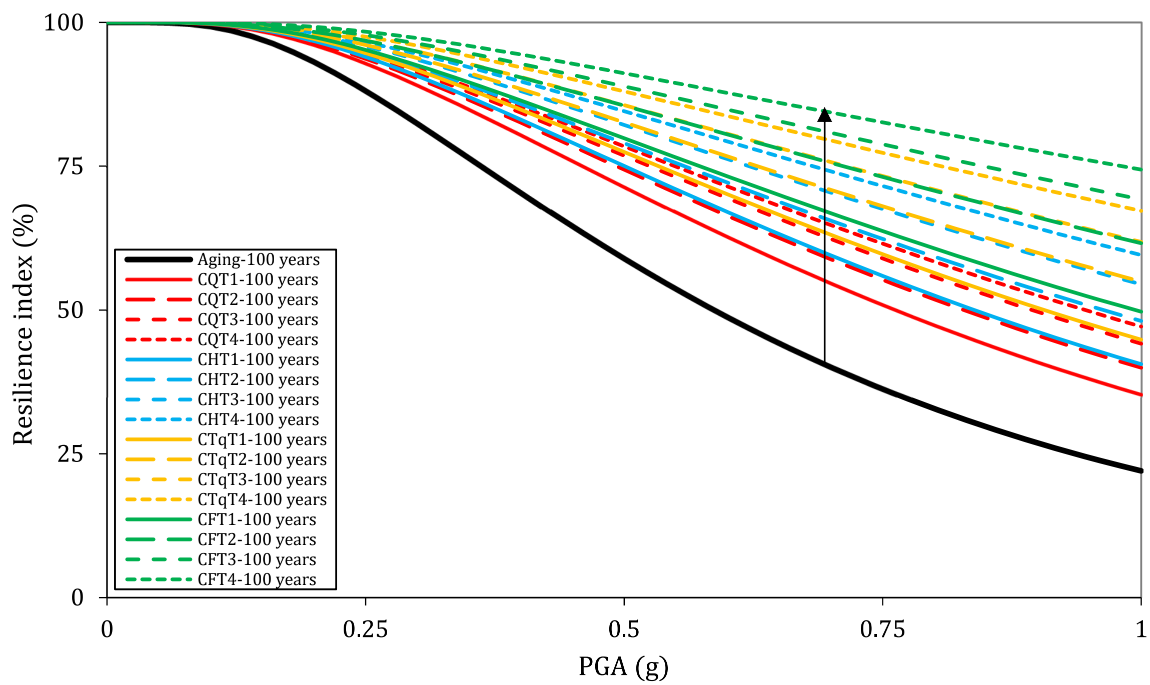

(d)

Fig. 10. Seismic time-dependent resilience curve right after an event for (a) non-retrofitted, (b) steel jacketing, (c) CFRP jacketing at the intact state (0 year aging), and (d) CFRP jacketing at the end of service life (100 years aging) under corrosion.

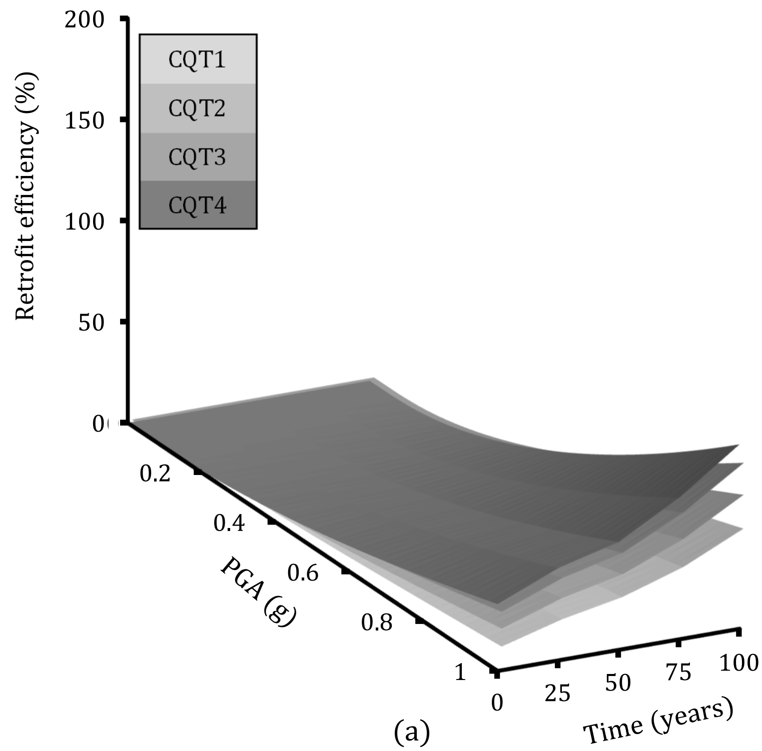
200
150
100
50
0
Retrofit efficiency (%)
CQT1
CQT2
CQT3
CQT4
0.2
0.4
0.6
0.8
1
PGA (g)
0
25
50
75
100
Time (years)

(a)

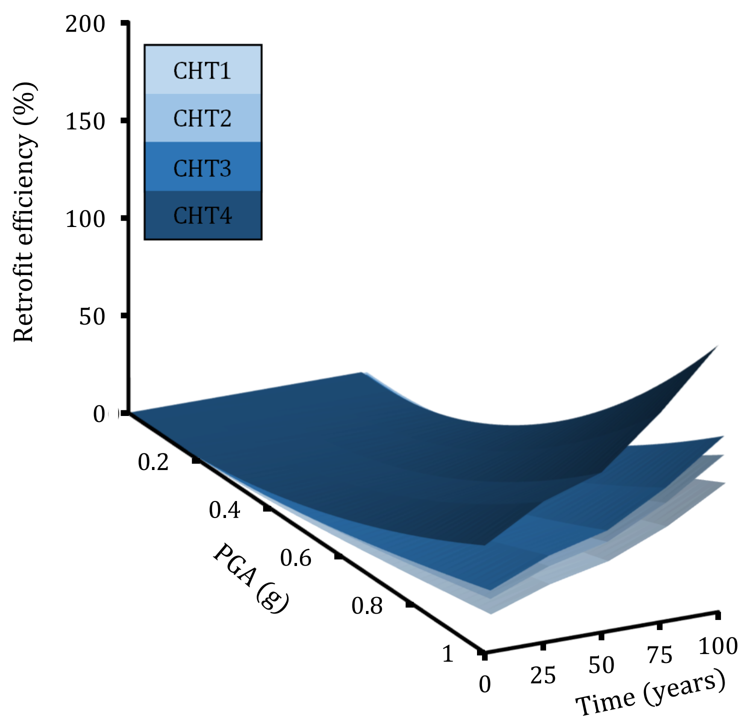
200
150
100
50
0
Retrofit efficiency (%)
CHT1
CHT2
CHT3
CHT4
0.2
0.4
0.6
0.8
1
PGA (g)
0
25
50
75
100
Time (years)

(b)

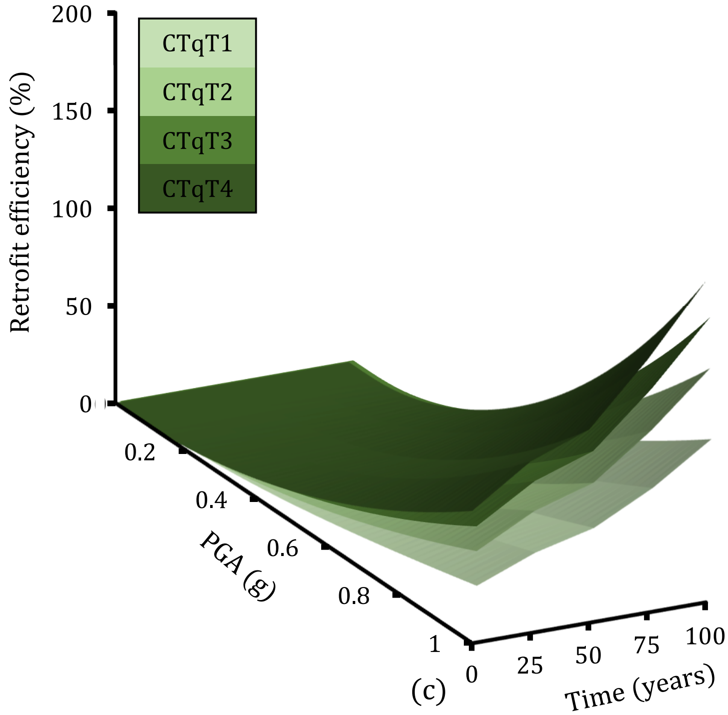

(c)

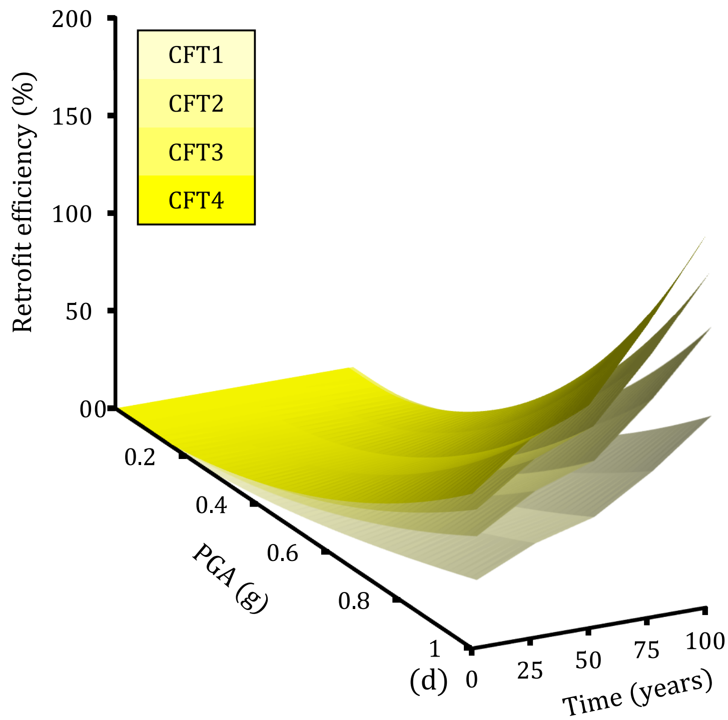

(d)

Fig. 11. Retrofit efficiency values of seismic time-dependent resilience for (a) CQT1-T4, (b) CHT1-T4, (c) CTqT1-T4, and (d) CFT1-T4 jacketing considering differing aging years.

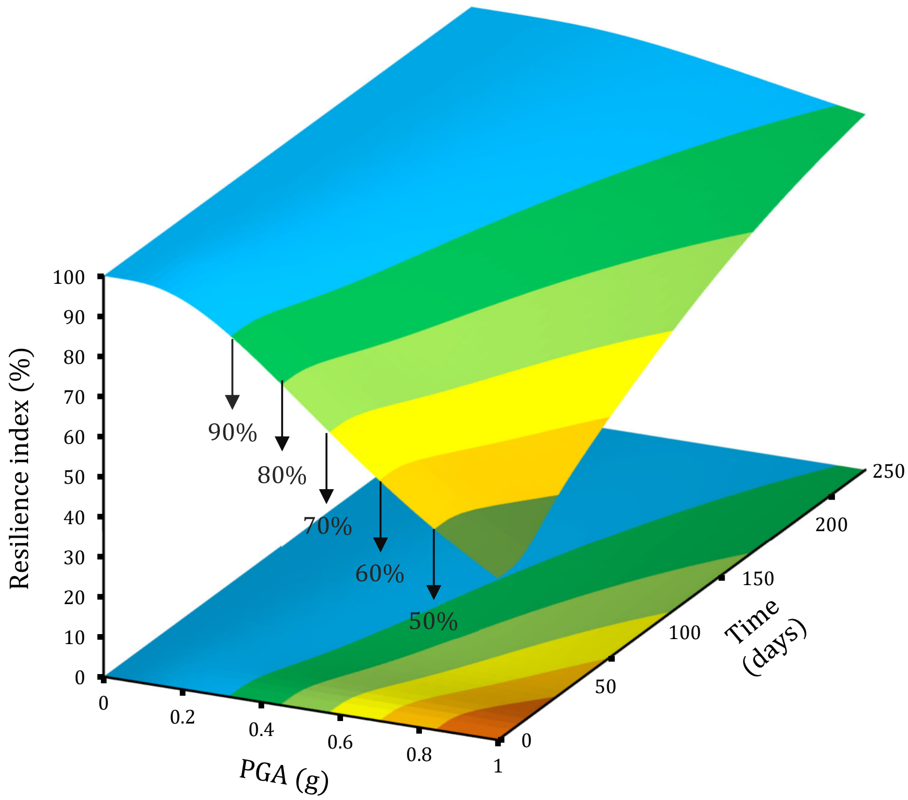
100
90
80
70
60
50
40
30
20
10
0
Resilience index (%)
90%
80%
70%
60%
50%
0
0.2
0.4
0.6
0.8
1
PGA (g)
0
50
100
150
200
250
Time (days)

(a)#

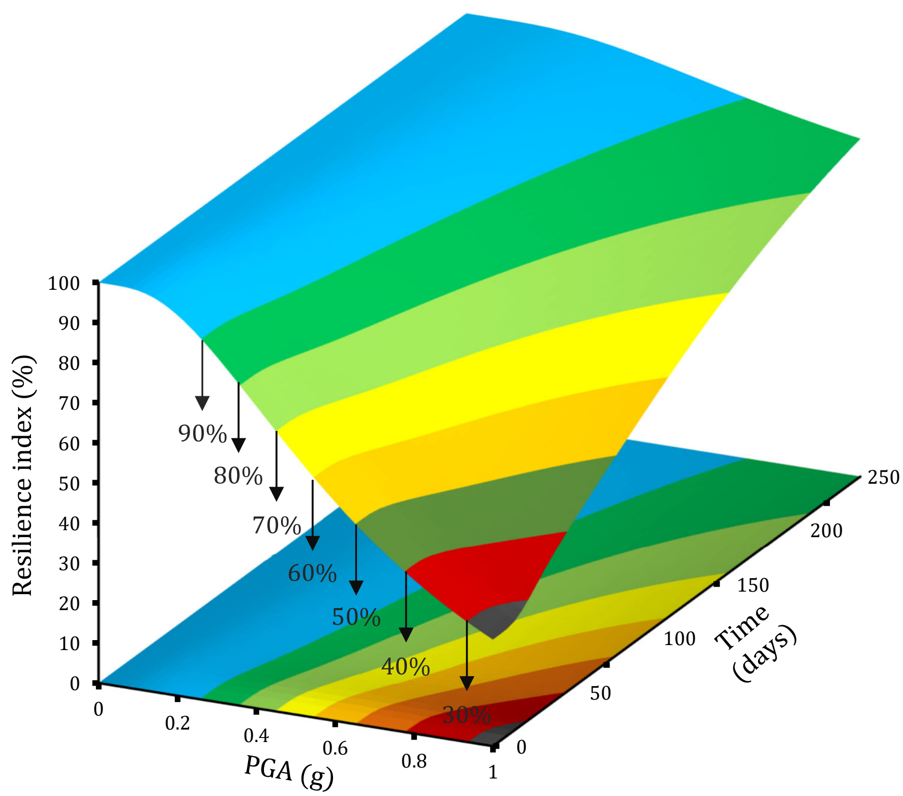
100
90
80
70
60
50
40
30
20
10
0
Resilience index (%)
90%
80%
70%
60%
50%
40%
30%
0
0.2
0.4
0.6
0.8
1
PGA (g)
0
50
100
150
200
250
Time (days)

(b)#

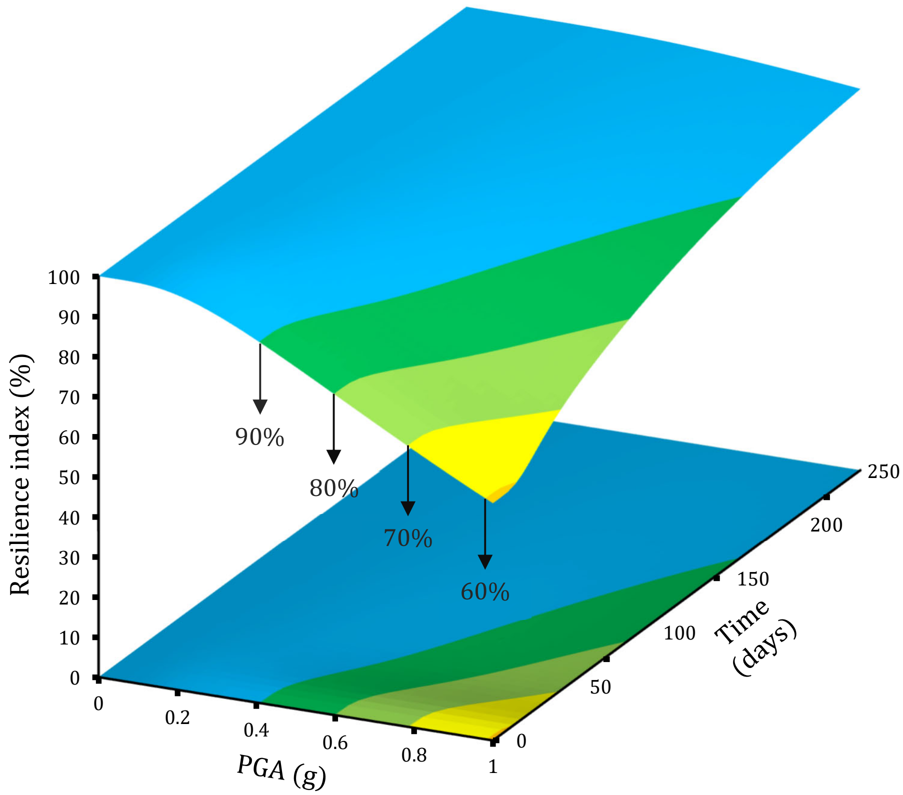

Resilience index (%)
100
90
80
70
60
50
40
30
20
10
0
90%
80%
70%
60%
0
0.2
0.4
0.6
0.8
1
PGA (g)
0
50
100
150
200
250
Time (days)

(c)#

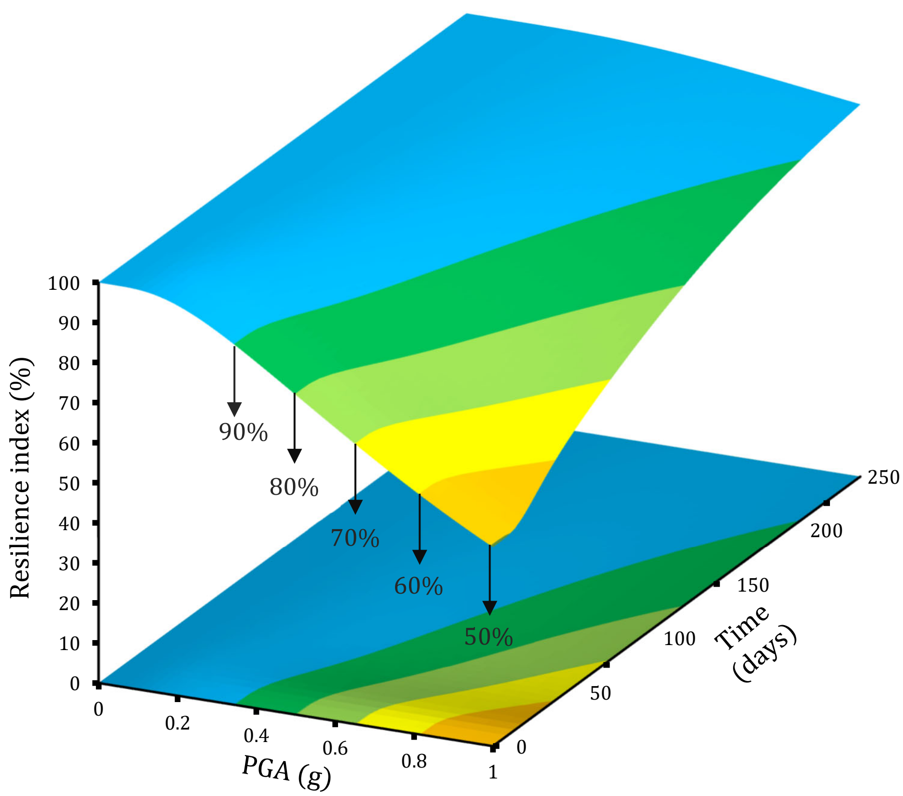

Resilience index (%)
100
90
80
70
60
50
40
30
20
10
0
90%
80%
70%
60%
50%
0
0.2
0.4
0.6
0.8
1
PGA (g)
0
50
100
150
200
250
Time (days)

(d)#

Fig. 12. Seismic time-dependent resilience surface in harmony with recovery path for (a) pristine non-retrofitted bridge, (b) 100 years aging non-retrofitted bridge, (c) CFT4 jacketing with 0 year aging, and (d) CFT4 jacketing at the end of service life (100 years aging) under corrosion.

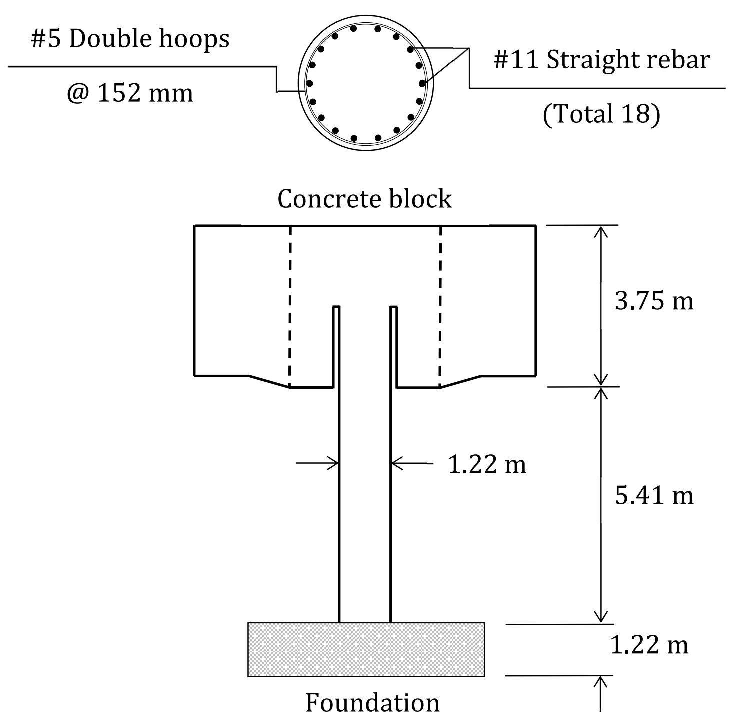

(a)

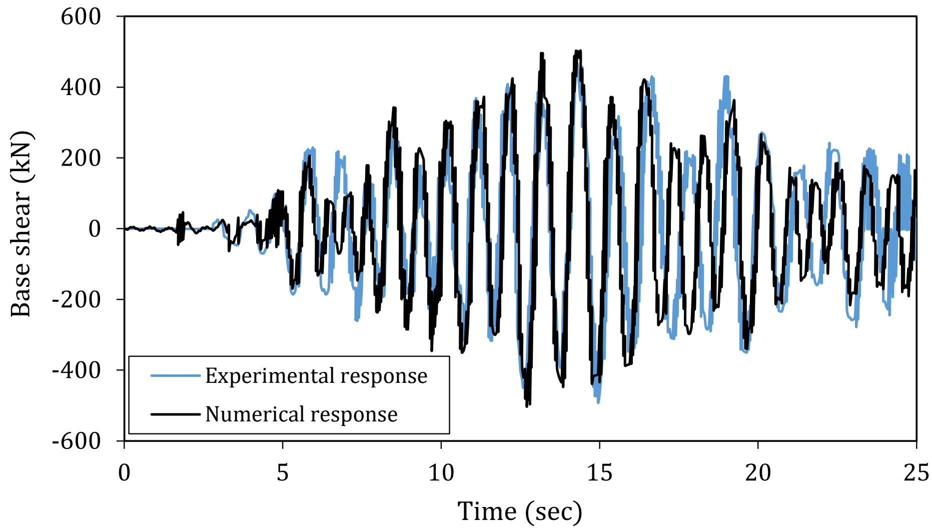

(b)

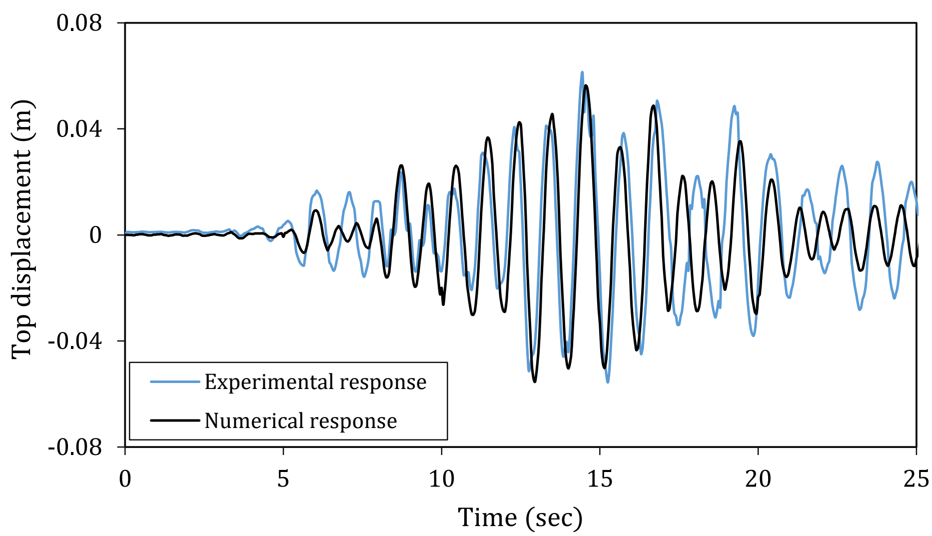

(c)

Fig. A1. General view of (a) a full-scale tested reinforced concrete bridge pier [91]. The numerical and experimental (b) base shear and (c) top displacement caused by the seismic record used in Ref. [91].

Table 1. Threshold of seismic damage-dependent recovery path and the statistical information for the required time of each damage state [35]

Damage state (DS_k)	Recovery path description	Recovery time (Days)			
		Log-normal mean (Lognormal standard deviation)			
		T_{ins}	T_{mob}	$T_{d\&c}$	T_{rep}
Minor	$T_{ins} + T_{d\&c} + T_{rep}$	4 (3.6)	- (-)	30 (27.4)	0.6 (0.6)
Moderate	$T_{ins} + T_{mob} + T_{d\&c} + T_{rep}$	4 (3.6)	45 (41.0)	40 (36.5)	2.5 (2.7)
Major	$T_{ins} + T_{mob} + T_{d\&c} + T_{rep}$	4 (3.6)	45 (41.0)	50 (45.6)	75 (42)
Collapse	$T_{ins} + T_{mob} + T_{d\&c} + T_{rep}$	4 (3.6)	45 (41.0)	60 (54.7)	230 (110)

Table 2. Threshold of damage state quantities prescribed by FEMA [33]

Bridge components	EDP (Physical phenomenon)	Cracking and spalling		Moderate cracking and spalling		Degradation without collapse		Failure leading to collapse		Ref. [33]
		Minor damage state (DS_1)		Moderate damage state (DS_2)		Major damage state (DS_3)		Collapse damage state (DS_4)		
		μ_k	σ_k	μ_k	σ_k	μ_k	σ_k	μ_k	σ_k	
Bridge piers	Displacement ductility, μ_d	1	0.73	1.2	0.61	1.76	0.74	4.76	0.77	Ref. [43-44]
Isolation bearings	Shear strain, γ (%)	100	0.79	150	0.68	200	0.73	250	0.66	Ref. [43-44]
Abutments	Active displacement, δ (mm)	9.75	0.25	37.9	0.25	77.2	0.46	N/A	N/A	Ref. [45-46]
	Passive displacement, δ (mm)	37	0.25	146	0.25	N/A	N/A	N/A	N/A	Ref. [45-46]

Table 3. The retrofitting strategies for jacketing RC bridge piers considered in this study

Retrofitting strategy name	Thicknesses of each material (mm)	Arrangements for each material	Materials
CFT1	2 plies × 1.24 mm	F (Full): 100% of all piers are jacketed	CFRP: Carbon Fiber-Reinforced Polymer
CFT2	4 plies × 1.24 mm		
CFT3	7 plies × 1.24 mm		
CFT4	10 plies × 1.24 mm		
CTqT1	2 plies × 1.24 mm	Tq (Three quarter): 75% of all piers are jacketed	
CTqT2	4 plies × 1.24 mm		
CTqT3	7 plies × 1.24 mm		
CTqT4	10 plies × 1.24 mm		
CHT1	2 plies × 1.24 mm	H (Half): 50% of all piers are jacketed	
CHT2	4 plies × 1.24 mm		
CHT3	7 plies × 1.24 mm		
CHT4	10 plies × 1.24 mm		
CQT1	2 plies × 1.24 mm	Q (Quarter): 25% of all piers are jacketed	
CQT2	4 plies × 1.24 mm		
CQT3	7 plies × 1.24 mm		
CQT4	10 plies × 1.24 mm		
GFT1	2 plies × 1.27 mm	F (Full): 100% of all piers are jacketed	GFRP: Glass Fiber-Reinforced Polymer
GFT2	4 plies × 1.27 mm		
GFT3	7 plies × 1.27 mm		
GFT4	10 plies × 1.27 mm		
GTqT1	2 plies × 1.27 mm	Tq (Three quarter): 75% of all piers are jacketed	
GTqT2	4 plies × 1.27 mm		
GTqT3	7 plies × 1.27 mm		
GTqT4	10 plies × 1.27 mm		
GHT1	2 plies × 1.27 mm	H (Half): 50% of all piers are jacketed	
GHT2	4 plies × 1.27 mm		
GHT3	7 plies × 1.27 mm		
GHT4	10 plies × 1.27 mm		
GQT1	2 plies × 1.27 mm	Q (Quarter): 25% of all piers are jacketed	
GQT2	4 plies × 1.27 mm		
GQT3	7 plies × 1.27 mm		
GQT4	10 plies × 1.27 mm		
SFT1	9.53 mm	F (Full): 100% of all piers are jacketed	Steel
SFT2	12.7 mm		
SFT3	19.05 mm		
SFT4	25.40 mm		
STqT1	9.53 mm	Tq (Three quarter): 75% of all piers are jacketed	
STqT2	12.7 mm		
STqT3	19.05 mm		
STqT4	25.40 mm		
SHT1	9.53 mm	H (Half): 50% of all piers are jacketed	
SHT2	12.7 mm		
SHT3	19.05 mm		
SHT4	25.40 mm		
SQT1	9.53 mm	Q (Quarter): 25% of all piers are jacketed	
SQT2	12.7 mm		
SQT3	19.05 mm		
SQT4	25.40 mm		

Table 4. Material properties used in the finite element analysis

Material	Mechanical property	Value
Concrete	Compressive strength (MPa)	35
	Tensile strength (MPa)	3.5
	Strain at peak stress (%)	0.2
Steel (bar)	Modulus of elasticity (GPa)	200
	Yield strength (MPa)	400
	Strain hardening parameters (%)	0.5
CFRP	Tensile strength (MPa)	930
	Tensile modulus (GPa)	89.6
	Ultimate elongation (%)	0.98
	Ply thickness (mm)	1.24
Steel (jacketing)	Modulus of elasticity (GPa)	200
	Ultimate tensile strength (MPa)	250
GFRP	Tensile strength (MPa)	587
	Tensile modulus (GPa)	27.4
	Ultimate elongation (%)	2.3
	Ply thickness (mm)	1.3

Table 5. The selected strong ground motions

Record No.	Earthquake	Year	Station Name	Magnitude	R rupture (km)	PGA (g)	Focal Mechanism
1	Kobe Japan	1995	Nishi-Akashi	6.9	7.08	0.498	Strike-slip
2	Northridge	1994	Sylmar - Converter Sta East	6.69	5.19	0.963	Reverse
3	Chichi Taiwan	1999	CHY080	7.62	2.69	0.953	Reverse oblique
4	Erzincan Turkey	1992	Erzincan	6.69	4.38	0.488	Strike-slip
5	Loma Prieta	1989	Corralitos	6.93	3.85	0.662	Reverse oblique
6	Helena Montana	1935	Carroll College	6	2.86	0.196	Strike-slip
7	Nahanni Canada	1985	Site 1	6.76	9.6	1.019	Reverse
8	Corinth Greece	1981	Corinth	6.6	10.27	0.272	Normal oblique
9	Norcia Italy	1979	Cascia	5.9	4.64	0.213	Normal
10	Izmir Turkey	1977	Izmir	5.3	3.21	0.41	Normal
11	Northern California	1941	Ferndale City Hall	6.4	44.52	0.115	Strike-slip
12	San Fernando	1971	Fairmont Dam	6.61	25.58	0.111	Reverse
13	Tabas Iran	1978	Boshrooyeh	7.35	24.07	0.106	Reverse
14	Imperial Valley	1979	Calipatria Fire Station	6.53	23.17	0.129	Strike-slip
15	Friuli Italy	1976	Codroipo	6.5	33.32	0.091	Reverse
16	Victoria Mexico	1980	SAHOP Casa Flores	6.33	39.1	0.1	Strike-slip
17	Chichi Taiwan	1999	CHY002	7.62	26.81	0.147	Reverse oblique
18	Coalinga	1983	Cantua Creek School	6.36	23.78	0.288	Reverse
19	Kern County	1952	Taft Lincoln School	7.36	38.42	0.18	Reverse
20	Northern California	1954	Ferndale City Hall	6.5	26.72	0.203	Strike-slip

Table 6. Descriptors of Lognormal random variables affecting the corrosion deterioration of RC piers [77]

Descriptor	Unit	Log-normal mean	Coefficient of variation
Cover depth (x)	cm	3.810	0.20
Diffusion coefficient (D_c)	cm^2/year	1.290	0.10
Surface chloride concentration (C_0)	wt % concrete	0.100	0.10
Critical chloride concentration (C_{cr})	wt % concrete	0.040	0.10
Rate of corrosion (r_{corr})	mm/year	0.127	0.30

Note: wt % concrete = percent by weight of concrete.

Table 7. Lognormally distributed functions for resilience estimation right after a seismic hazard event along service life for FT1 strategies

Year	Non-retrofitted	Steel	GFRP	CFRP
0	$100\% - LN(0.83, 0.72)$	$100\% - LN(1.03, 0.78)$	$100\% - LN(1.06, 0.80)$	$100\% - LN(1.23, 0.82)$
25	$100\% - LN(0.76, 0.71)$	$100\% - LN(0.96, 0.73)$	$100\% - LN(1.01, 0.81)$	$100\% - LN(1.18, 0.81)$
50	$100\% - LN(0.71, 0.69)$	$100\% - LN(0.94, 0.75)$	$100\% - LN(0.99, 0.79)$	$100\% - LN(1.16, 0.78)$
75	$100\% - LN(0.64, 0.67)$	$100\% - LN(0.82, 0.72)$	$100\% - LN(0.89, 0.73)$	$100\% - LN(1.08, 0.78)$
100	$100\% - LN(0.56, 0.68)$	$100\% - LN(0.76, 0.77)$	$100\% - LN(083, 0.75)$	$100\% - LN(1.01, 0.80)$

Note: $LN(\mu, \sigma)$ refers to Lognormal distribution with parameters μ and σ, which are the mean (in PGA) and standard deviation of the corresponding distribution, respectively.

Table 8. Predictive exponential functions of logistic regression for quantifying the percentage increase in median of resilience log-normal distribution

Strategy	Ratio [1*, 2*]	Steel	GFRP	CFRP
Quarter	T_i/T_1	$3.43e^{0.50T_i}$	$3.76e^{0.53T_i}$	$5.066e^{0.55T_i}$
Half		$4.84e^{0.57T_i}$	$6.36e^{0.51T_i}$	$9.24e^{0.56T_i}$
Three quarters		$7.43e^{0.54T_i}$	$9.11e^{0.54T_i}$	$12.89e^{0.54T_i}$
Full		$9.91e^{0.56T_i}$	$11.57e^{0.56T_i}$	$16.88e^{0.57T_i}$
T_1	A_i/A_1	$3.51e^{0.48A_i}$	$3.91e^{0.51A_i}$	$4.85e^{0.57A_i}$
T_2		$4.85e^{0.58A_i}$	$6.20e^{0.56A_i}$	$8.82e^{0.58A_i}$
T_3		$6.54e^{0.62A_i}$	$8.16e^{0.58A_i}$	$11.55e^{0.60A_i}$
T_4		$8.764e^{0.60A_i}$	$9.43e^{0.61A_i}$	$14.953e^{0.59A_i}$

Note 1: where $T_i \in \{2, 3, 4\}$ is the thickness category (2-4 represent 4, 7, and 10 plies of CFRP/GFRP or 12.7, 19.05 and 25.40 mm of steel jacketing)

Note 2: where $A_i \in \{2, 3, 4\}$ is the arrangement category (2-4 represent Half, Three quarter, and Full retrofit arrangement)